

1 Highlights

2 **Accurate Determination of the Electron Spin Polarization In Mag-** 3 **netized Iron and Nickel Foils for Møller Polarimetry**

4 D. C. Jones, J. Napolitano, W. Henry, D. G. Gaskell, S. Malace, D. E. King,
5 P. Souder, K. Paschke

6 • Research highlight 1

7 • Research highlight 2

8 Accurate Determination of the Electron Spin
9 Polarization In Magnetized Iron and Nickel Foils for
10 Møller Polarimetry

11 D. C. Jones^{a,*}, J. Napolitano^a, W. Henry^b, D. G. Gaskell^b, S. Malace^b, D.
12 E. King^c, P. Souder^c, K. Paschke^d

13 ^a*Temple University, Philadelphia, PA, 19122*

14 ^b*Jefferson Lab, Newport News, VA 23606*

15 ^c*Syracuse University, Syracuse, NY 13244*

16 ^d*University of Virginia, Charlottesville, VA 22903*

17 **Abstract**

18 The Møller polarimeter in Hall A at Jefferson Lab in Newport News, VA, has
19 provided reliable measurements of electron beam polarization for the past two
20 decades. Past experiments have typically required polarimetry at the sev-
21 eral percent level of absolute uncertainty which the Møller polarimeter has
22 delivered. However, the upcoming proposed experimental program including
23 MOLLER and SoLID have stringent requirements on beam polarimetry pre-
24 cision at the level of 0.4%[1, 2], requiring a systematic rethinking of all the
25 contributing uncertainties.

26 Møller polarimetry uses the double polarized scattering asymmetry of a
27 polarized electron beam on a target with polarized atomic electrons. The
28 target is a ferromagnetic material magnetized to align the spins in a given
29 direction. In Hall A, the target is a pure iron foil aligned perpendicular to
30 the beam and magnetized out of plane parallel or antiparallel to the beam
31 direction. The acceptance of the detector is engineered to collect scattered
32 electrons close to 90° in the center of mass frame where analyzing power is a
33 maximum.

One of the leading systematic errors comes from determination of the target foil polarization. Polarization of a magnetically saturated target foil requires knowledge of both the saturation magnetization and g' , the electron g -factor which includes components from both spin and orbital angular momentum from which the spin fraction of magnetization is determined. Target foil polarization has been previously addressed in a 1997 publication “A pre-

^{*}Corresponding author
Preprint submitted to Nuclear Inst. and Methods in Physics Research, A, February 22, 2022
Email address: donald.d.jones@temple.edu (D. C. Jones)

cise target for Møller polarimetry” by deBever *et. al* [3] at a level of precision sufficient for experiments up to this point. Several shortcomings with the previous published value require revisiting the result prior to MOLLER. This paper utilizes the existing world data to provide a best estimate for target polarization for both Nickel and Iron foils including uncertainties in magnetization, high-field and temperature dependence, and fractional contribution to magnetization from orbital effects. We determine the foil electron spin polarization at 294 K to be 0.08020 ± 0.00018 (@4 T applied field) for iron and 0.018845 ± 0.000053 (@2 T applied field) for nickel. We conclude with a brief discussion of additional systematic uncertainties to Møller polarimetry using this technique.

34 *Keywords:*

35 1. Introduction to Møller polarimetry

36 As its name denotes, Møller polarimetry utilizes the analyzing power
 37 of polarized electron-electron scattering to determine the polarization of an
 38 electron beam. The polarized target is usually composed of iron or a highly
 39 ferromagnetic material. Elastically scattered events (beam electrons from
 40 atomic electrons) produce back-to-back electrons in the center of mass frame.
 41 If both are detected in coincidence background contributions can be signifi-
 42 cantly reduced.

Following the analysis in [4], where the center of mass energy of the e^-e^- pair $E_{CM} \gg m_e$, Møller (electron-electron) scattering at tree level in the electron-electron center of mass (CM) system is given by

$$\frac{d\sigma}{d\Omega_{cm}} = \frac{\alpha^2}{4E_{CM}^2} \frac{(3 + \cos^2 \theta)^2}{\sin^4 \theta} \left[1 - \right. \\ \left. P_\ell^{\text{targ}} P_\ell^{\text{beam}} A_\ell(\theta) - P_t^{\text{targ}} P_t^{\text{beam}} A_t(\theta) \cos(2\phi - \phi_{\text{beam}} - \phi_{\text{targ}}) \right] \quad (1)$$

43 where the subscripts t and ℓ refer to transverse and longitudinal polarization
 44 respectively. The CM scattering angle is θ and the azimuthal angle of the
 45 target (beam) polarization with respect to the electron beam is $\phi_{\text{targ(beam)}}$.
 46 The analyzing powers for longitudinal and transverse polarization are given
 47 by

$$A_\ell(\theta) = \frac{(7 + \cos^2 \theta) \sin^2 \theta}{(3 + \cos^2 \theta)^2} \quad \text{and} \quad A_t(\theta) = \frac{\sin^4 \theta}{(3 + \cos^2 \theta)^2}. \quad (2)$$

At $\theta = 90^\circ$, A_ℓ is at its maximum value of $7/9$ which is a factor of 7 larger than A_t giving Møller polarimetry much more sensitivity to longitudinal polarization. The optics of the Møller polarimeter in Hall A are tuned to accept events near this maximum analyzing power for longitudinal polarization. The Møller polarimeter in Hall A with its Fe foil polarized “out of plane” in the beam direction ($P_t^{\text{targ}} = 0$) is designed to measure the longitudinal polarization and be insensitive to the transverse polarization. Nevertheless, if the foil or magnetizing coils are not properly aligned and a transverse foil polarization develops, a non-negligible component of transverse asymmetry could in principle arise. In the ensuing discussion it will be assumed that the foil is properly aligned such that $P_t^{\text{targ}} = 0$ and this term will be neglected.¹

Integrating the cross section over the acceptance of the detector gives

$$\sigma \propto 1 - P_\ell^{\text{targ}} P_\ell^{\text{beam}} A_{zz},$$

where $A_{zz} = \langle A_t(\theta) \rangle$, the acceptance-weighted analyzing power. We can now see that the left-right scattering asymmetry A_{LR} is then given by

$$A_{LR} = \frac{\sigma_R - \sigma_L}{\sigma_R + \sigma_L} = P_\ell^{\text{targ}} P_\ell^{\text{beam}} A_{zz}, \quad (3)$$

where $\sigma_{L(R)}$ are the cross sections for left (right) helicity electrons. Implicit in this form is the assumption that P_ℓ^{beam} is the same for both helicity states. If A_{zz} and the target polarization P_ℓ^{targ} are known, the beam polarization can be determined from the measured scattering asymmetry.

In the approximation where the target electrons are at rest and the beam energy is large compared to the electron rest mass m_e , the relationship between the lab momentum of the scattered electron, p' , and the center of mass scattering angle θ is given by

$$p' = \frac{p_b}{2} (1 + \cos \theta), \quad (4)$$

¹We can approximate the relative size of this term to justify our neglect of it. Longitudinal polarization at JLab can be adjusted for experiments to within $\pm 2^\circ$ of uncertainty, leaving a maximum P_t^{targ} of 0.035. Assuming an anomalously large transverse component of the target polarization due to misalignment of 5% and a transverse analyzing power that is approximately 1/7 that of the longitudinal gives a maximum transverse polarization contribution (i.e. for a beam and target polarization at the same azimuthal angle) that is 0.025% that of the longitudinal term.

where p_b is the electron beam momentum. Thus momentum analyzing the Møller scattered electrons also analyzes in θ . Single arm Møller polarimeters leverage this characteristic to reduce potentially overwhelming backgrounds arising from Mott scattering from the nucleus. Using a narrow aperture in ϕ to select the scattering plane and a dipole to momentum analyze the scattering events perpendicular to the scattering plane produces a characteristic Møller “stripe” downstream of the dipole. Converting to the lab scattering angle and in the absence of other focussing optics, and using the small angle approximation yield the following relationship between θ_{Lab} and momentum:

$$\theta_{\text{Lab}}^2 = 2m_e c \left(\frac{p_b - p'}{p' p_b} \right). \quad (5)$$

The typical quadratic curvature of this Møller stripe is a direct result of this relationship.

1.1. The Møller polarimeter in Hall A at Jefferson Lab

Part of the standard equipment in Hall A at Jefferson Lab is the Møller polarimeter, used to measure the electron beam polarization in the Hall. Most experiments in the past have had polarization requirements at the several percent uncertainty level easily attained by the Møller. Two recent experiments, PREX-2[5] and CREX, have reached $<0.9\%$ uncertainty for Møller polarimetry. However, MOLLER and SoLID, the future parity violation experiments planned for Hall A in 2025 and beyond, require uncertainty in electron polarization at $\pm 0.4\%$, a record-breaking level of precision that requires rethinking all the possible sources of systematic error. This paper is designed to address specifically the uncertainty associated with target foil polarization for these experiments, but has obvious value for other Møller polarimeters around the world. Where appropriate, we will provide the means to extrapolate these results to other polarimeters with different designs and operating parameters.

The polarimeter in Hall A is designed to take advantage of both the dipole momentum selection and the coincidence of dual arm detection to further reduce backgrounds. A simple schematic of the Hall A polarimeter is shown in Fig. 1 illustrating the key features. This polarimeter design adds to the essential elements 4 quadrupoles and an additional horizontal constraint due to the narrow apertures through the dipole. The quadrupoles are used to focus a distribution of Møller pairs roughly symmetric about the 90 degree center of mass through the dipole onto the detector. The additional focusing

of the quadrupoles inverts the expected typical curvature of the Møller stripe on the detector plane as illustrated in Fig. 1.

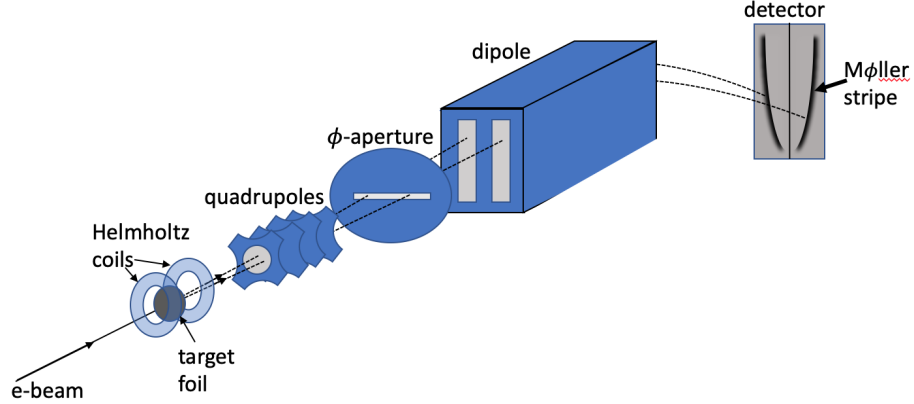


Figure 1: Simplified schematic showing the key features of the Møller polarimeter setup in Hall A. The electron beam scatters from a polarized foil target. Quadrupole magnets then focus the events of interest through the dipole magnet. An aperture at the front of the dipole limits the ϕ -acceptance, defining a horizontal scattering plane. Two left-right symmetric narrow slits in the dipole, momentum analyze the scattered electron pairs bending them down onto the detector plane producing characteristic Møller stripes.

106

107 2. Foil Target Polarization

108 In the context of Møller polarimetry, target polarization is produced using a strong magnetic field to align electron spins in ferromagnetic materials. 109 Magnetization, \mathbf{M} , is defined as the magnetic dipole moment per unit volume or in certain contexts, per unit mass. The magnetization provides the 110 magnetic field contributed by a material and relates the flux density \mathbf{B} to the auxiliary field \mathbf{H} as follows: 111 112 113

$$\mathbf{B} = \mathbf{H} + 4\pi\mathbf{M}.$$

114 Note that this is in Gaussian units which are used throughout this document.

115 The Møller polarimeter target in Hall A consists of a set of thin foils 116 mounted on a target ladder and magnetized out of plane parallel (or antiparallel) to the beam trajectory by a set of superconducting Helmholtz coils. 117 The superconducting magnet used to polarize the target foils was built by 118 American Magnetics Inc. The field at the center of the coils is horizontal and 119

Table 1: Properties of the three ferromagnetic elements. This manuscript focusses on the absolute uncertainties on M_0 and g' .

	Fe	Co	Ni
Z	26	27	28
Atomic Mass (μ)	55.845(2)	58.933194(4)	58.6934(4)
Electron Configuration	[Ar]4s ² 3d ⁶	[Ar]4s ² 3d ⁷	[Ar]4s ² 3d ⁸
Unpaired Electrons	2.2	1.72	0.6
Density near r.t. (g/cm ³)	7.874	8.900	8.902
M_0 at 0 K (emu/g)	222	164	58.6
g'	1.92	1.85	1.84
Curie Temperature (K)	1043	1400	631
Stable Isotopes	⁵⁴ Fe (5.85%) ⁵⁶ Fe (91.75%) ⁵⁷ Fe (2.12%) ⁵⁸ Fe (0.28%)	⁵⁹ Co (100%)	⁵⁸ Ni (68.08%) ⁶⁰ Ni (26.22%) ⁶¹ Ni (1.14%) ⁶² Ni (3.64%) ⁶⁴ Ni (0.93%)

120 along the beam-line axis. The maximum field at the center is rated at 5 T,
121 although we do not typically run above 4 T.

122 The three ferromagnetic elements, Fe, Co and Ni are the obvious choices
123 for foil targets due to their relatively high magnetization and the precision
124 with which their magnetizations are known. A list of the main properties
125 of these elements is given in Table 1. The magnetization of Fe and Ni are
126 both known to high accuracy ($\sim 0.2\%$), but the low Curie temperature of Ni
127 makes it susceptible to large (percent level) corrections from target heating
128 effects. There are fewer published measurements of high precision on Co
129 than on the other two ferromagnetic elements.

130 Møller polarimetry requires finding the average target electron polariza-
131 tion; however, magnetization measures the magnetic moment of the whole
132 atom including the orbital and spin magnetic moments. Since we only want
133 the spin component we need to find the fraction of the magnetization that
134 comes from spin. This is typically determined from precise measurements of
135 the gyromagnetic ratio (the ratio of a material's magnetization to its angu-
136 lar momentum) of an elemental sample. Thus, the final error on the target
137 polarization will include uncertainties on both the determination of magne-

138 tization and of the spin fraction. In the following sections we look at each
 139 of the three elements and determine the systematic uncertainty associated
 140 with using each as a target materials. The primary issues to be dealt with
 141 are follows:

- 142 • From 1930-1980 many precise measurements have been made of the
 143 magnetization and gyromechanical properties of these elements; how-
 144 ever, they do not necessarily agree within error. Sometimes the errors
 145 quoted are not realistic given the systematic disagreement in the data.
 146 The sources of systematic difference are often not known and yet results
 147 are averaged together and the final error estimated from the variance
 148 of the data.
- 149 • No mention is made of the nuclear contribution to the magnetic mo-
 150 ment. The nuclear magneton is smaller than the Bohr magneton by a
 151 factor of $m_e/m_p \sim 0.05\%$. Fortunately, the main isotopes that make up
 152 iron and nickel are even-even and have spinless nuclei, but for Co the
 153 average is 4.6 nuclear magnetons making the contribution potentially
 154 above the 0.1%.
- 155 • Measurements of magnetization and gyromechanical properties are not
 156 made at the same applied field and temperature where the Møller po-
 157 larimeter operates, necessitating corrections to account for these differ-
 158 ences. The corrections must be known to sufficient accuracy and the
 159 conditions under which the measurements were taken must be known.
- 160 • Through the past century measurement of constants have become more
 161 precise and have changed. Examples of constants used in determining
 162 quoted magnetization and gyromagnetic data in the literature are the
 163 density of elements, the charge to mass ratio of the electron, and the
 164 Bohr magneton. Different groups use different values. Sometimes the
 165 values of constants used in calculations (eg. the Bohr magneton) are
 166 assumed to be known and are not given.
- 167 • Experiments measuring properties of these ferromagnetic elements used
 168 different levels of purity. It is not clear what uncertainty should be
 169 assigned to account for the effects of impurities.
- 170 • In many publications, the data are only shown as plots and the values
 171 of the measurements are not provided. The values must be extracted

with plot digitization software.

- In order to compare magnetization data taken with different sample shapes, the applied field must be converted to the internal field, H_{int} . This conversion is not always possible if the data are not given in terms of H_{int} or the sample shape and dimensions are not provided so that this conversion from applied to internal field can be made.

2.1. Determining Saturation Magnetization

Target polarization is determined from measurements of the saturation magnetization. Another term used in the literature is “spontaneous magnetization,” which, as the name implies, refers to the magnetic moment of a material that spontaneously arises with no applied field. In ferromagnetic materials the magnetic moments of the electrons tend to spontaneously align in a given direction. However, due to energy considerations, domains tend to form in such a way that the total spin averaged across many domains at the macroscopic level is far below the saturation level and may be zero. In the presence of an applied magnetic field, the domain boundaries shift with enlarging domains having magnetic moments aligned along the direction of the field. As the applied field is increased, eventually the material will reach magnetic saturation where all the spins are aligned along the direction of the applied field. Thus, the saturation magnetization and the spontaneous magnetization are related quantities and spontaneous magnetization is numerically equal to the saturation magnetization at 0 K. Quoting from [6]: “Under a sufficiently high external magnetic field, the sample reaches saturation and represents a single-domain system oriented along this field direction. Therefore, the saturation magnetization can be considered to be equal (to) the spontaneous magnetization of one domain.” For a discussion of domain formation and saturation magnetization see Kittel’s Review paper from 1949[7].

2.1.1. Temperature and Field Dependence of Saturation Magnetization

Spontaneous magnetization is a function of temperature and applied field and for this reason it is often given as M_0 , the value of saturation magnetization extrapolated to zero applied field at $T = 0$ K. However, experiments measure the magnetization at temperatures above 0 K with non-zero applied fields. For temperatures well below the Curie temperature and low applied

207 fields, the magnetization has been shown to roughly follow the $T^{3/2}$ law of
 208 Bloch given as [8]

$$M_s(T) = M_0(1 - a_{3/2}T^{3/2}), \quad (6)$$

209 where M_0 is the saturation magnetization at 0 K and $a_{3/2}$ is an empirically
 210 determined constant.

211 This temperature-dependence of the saturation magnetization arises pri-
 212 marily from the presence of spin-waves which are traveling excitations of spin
 213 precessions about the magnetic field propagating through a material. Spin
 214 waves propagate via coupling between neighboring spins and are strongly
 215 temperature-dependent with thermal energy driving the excitations. Near
 216 absolute zero, spin waves are nearly absent and their increased effect with
 217 temperature causes saturation magnetization to decrease with temperature
 218 as the overall alignment of individual atomic moments with the applied field
 219 decreases. Increasing the applied field also decreases the effect of spin waves
 220 so that at high fields and low temperature their effect is diminished. For a
 221 more detailed discussion of spin waves see [9, 10, 11, 12].

222 At higher fields and temperatures not small compared to the Curie tem-
 223 perature additional terms are required beyond those included in Eq. 6. Free-
 224 man Dyson used an expansion in powers of T to parameterize the depen-
 225 dence of saturation magnetization on temperature and applied field[13, 10].
 226 Frederic Keffer building on the work of Dyson and others developed a more
 227 elaborate form of the expansion with terms depending on $T^{3/2}$, $T^{5/2}$, $T^{7/2}$
 228 and T^2 as well as the strength of the internal field[14]. The half-power terms
 229 in T arise from spin waves and the T^2 term accounts for the possibility of
 230 Stoner-type excitations from the band structure in metals[15].

231 This parameterization, while accounting for temperature and field depen-
 232 dence arising from spin waves, fails to account for the nearly linear high-field
 233 paramagnetic susceptibility of ferromagnets well above saturation as well as
 234 effects unique to each sample which prevent saturation and thought to arise
 235 from impurities, strains, anisotropy, domains and even the geometry of the
 236 sample[11]. Foner *et al.* divide magnetization data into three regions: 1. the
 237 low-field region approaching saturation where the aforementioned sample-
 238 dependent effects prevent saturation at the theoretical saturation value and
 239 create curvature unique to each sample in the M versus H_{int} curves just be-
 240 low saturation; 2. the high-field region above saturation where effects from
 241 spin waves and possible remnant anisotropy remain in addition to the high-
 242 field susceptibility; 3. and the ultra-high field region where magnetic phase

transitions may exist and which is not of interest here[11]. These considerations suggest that use of Keffer's parameterization may require additional terms to account for the linear high-field susceptibility as well as non-linear curvature in the approach to saturation.

Pauthenet performed an extremely precise measurement of the saturation magnetization of Fe and Ni as a function of both temperature and internal field from 0 to 17 T. Pauthenet claims the absolute scale in his measurements is known only to $\pm 0.5\%$ due to uncertainty in calibration but that relative uncertainty is at the 0.01% level, making his work an authoritative reference for high field corrections. Following the work of Keffer, he expressed the saturation magnetization M as a function of temperature and internal field, while adding a term linear in applied field, $\chi(T)$, to account for the known effect of high field susceptibility:[14, 12, 15]

$$M(H_{\text{int}}, T) = M_0 \left(1 - \sum_{s=\frac{3}{2}, \frac{5}{2}, \frac{7}{2}} a_s \frac{F(s, t_H)}{\xi(s)} T^s - a_2 T^2 \right) + \chi(T) H_{\text{int}}. \quad (7)$$

Here M_0 is the spontaneous magnetization at 0 K and zero applied field, $F(s, t_H) = \sum_{p=1}^{\infty} p^{-s} e^{-pt_H}$ is the Bose-Einstein integral function, and $t_H = g\mu_B H_{\text{int}}/k_B T$, where g is the Lande g-factor, μ_B is the Bohr magneton, and k_B is the Boltzmann constant. H_{int} is the internal field and $\xi(T)$ is the Riemann zeta function. Pauthenet fits this parameterization to his data to give numerical values for the coefficients, providing magnetization as a function of internal magnetic field and temperature (see Eq. 9, 10 and Table 1 from [12]). We use Pauthenet's numerical parameterization of magnetization as a function of internal field and temperature provided in Eqs. 9 and 10 of [12], to make corrections for differences in temperature and internal field.

It is important to note the difference between internal field and applied field. In a manner somewhat analogous to the internal electric field cancellation inside a dielectric, the applied magnetic field is partially cancelled inside a ferromagnetic sample. This can be viewed as being caused by magnetic charges moving to the boundaries of the sample in accordance with the direction of the magnetic field. Their displacement will enhance the field outside the sample while reducing it inside. The relationship between the internal field and the applied field is given by the following equation (in the cgs system)

$$H = H_{\text{int}} + \frac{4\pi M}{\rho}, \quad (8)$$

275 where H is the applied field, H_{int} is the internal field, M is the magnetization
 276 and ρ is a demagnetization constant that depends on the shape of the sample.
 277 Since the internal field is thus partially cancelled by the magnetization, $4\pi M$
 278 is sometimes referred to as the “demagnetizing field”.

279 Well below saturation, the internal field is nearly 0 due to the demagne-
 280 tizing field. In the literature, field-dependent corrections are often given as
 281 a function of internal field H_{int} not applied field H . Above saturation mag-
 282 netization, H_{int} is less than H by the saturation magnetization (21.58 kOe
 283 for iron and 6.2 kOe for nickel). There appear to be errors in the literature
 284 that stem from incorrect exchanges of applied field and internal field. For
 285 example, Eq. 3 from deBever *et al.* incorrectly interprets Pauthenet’s cor-
 286 rections as a function of flux density B instead of internal field. As a result,
 287 they calculate a correction from an applied field of 1 T to the final value of
 288 4 T. A 4 T field applied normal to a thin Fe foil such as they were discussing
 289 translates into an internal field of ~ 1.8 T for Fe foils, requiring a smaller
 290 correction. C. D. Graham also appears to confuse the two in Fig. 5 of [16]
 291 where he plots magnetization versus $1/H$ but combines data from multiple
 292 sources some of which are in terms of $1/H$ and others which are in terms of
 293 $1/H_{\text{int}}$.

294 2.1.2. Other Factors Affecting Magnetization Measurements

295 There are several issues to be aware of when trying to interpret magneti-
 296 zation values quoted in the literature.

297 **Shape anisotropy:** the magnetization depends upon the shape of the
 298 object. Needles are very easy to magnetize along their long axis but much
 299 more difficult along a direction perpendicular to it. Each shape has a charac-
 300 teristic demagnetizing factor ρ (see Eq. 8) that is a function of the direction
 301 of applied field (unless symmetry dictates otherwise). Perfect spheres have
 302 a demagnetizing factor of $1/3$. The demagnetizing factor for ellipsoids of ro-
 303 tation is a function of the ratio of the two axis lengths. Figure 2 shows the
 304 demagnetizing factor of ellipsoids of rotation as a function of the axis ratio
 305 where the applied magnetic field is along the axis R_z . A thin foil disk such
 306 as that used in the Møller polarimeter can be taken to a flattened ellipsoid
 307 with an axis ratio of ~ 0 . In this case the demagnetizing factor approaches
 308 unity[17].

309 **Crystal anisotropy:** the crystal structure of a material can create di-
 310 rections along which it is easier to magnetize. The direction along which
 311 magnetic saturation is reached with the smallest applied field is called the

easy axis of the crystal. Monocrystalline nickel, for example, has three different magnetization axes termed the [111], [110] and [100] axes, using standard Miller index notation, with [111] being the easy axis. Therefore, if one is using monocrystalline materials, the magnitude of the external field required to reach saturation will depend upon alignment of the crystal relative to the field. For polycrystalline materials there will be no preferred direction as a result of the random crystal orientations.

Crystal structure and phase changes: some crystals have more than one possible crystal structure with different magnetizations. Their history of heating/cooling and annealing can have an effect on their magnetic properties. Cobalt, for example, goes through a phase change when heated at 690 K going from a close-packed hexagonal to a face-centered cubic crystal structure above 690 K which is unstable below that temperature. However, the exact crystal structure below 690 K (and by extension the magnetization) depends upon the grain size and the annealing process used to prepare it[18].

Stesses and strains: stresses and strains in the material as well as porosity will affect how easily the material is magnetized. This can be seen particularly well by annealing, which often makes the material more easily magnetized[19].

2.1.3. *Measurements of Saturation Magnetization*

Although different methods are used to measure the saturation magnetization, they broadly break down into two categories. 1. Force method: a small ellipsoid sample of the element of interest is placed in a precisely determined field gradient. With a proper setup, the force on the sample by the magnetic field can be shown to be the product of the magnetic moment of the sample and the magnetic field gradient. Thus the magnetic moment of the sample is given as the force divided by the field gradient. Dividing by the mass of the sample gives the mass magnetization directly. A possible source of systematic error in this method is the use of standard weights and a balance to measure forces. Conversion from mass to force requires knowing the gravitational acceleration at the measurement location and relative uncertainty in this value translates directly into the final result. Of the magnetization measurements included in this study, only those by Crangle *et al.* utilized this method. 2. Induction method: a sample is placed into a magnetic field and its presence creates a magnetic moment that is measured in pickup coils. This directly measures volume magnetization and must be converted to mass magnetization by multiplying by density, introducing another

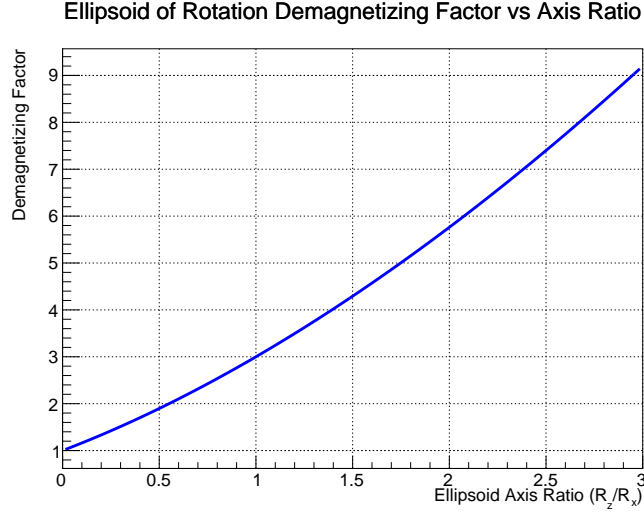


Figure 2: Demagnetizing factor for ellipsoids of rotation as a function of axis ratio for external magnetic field applied along the axis of rotation R_z . This plot uses equations 1a and 1b from [17].

349 potential source of systematic error.

350 Although the experimental methods can be thus broadly categorized, each
 351 individual experiment takes a slightly different approach to measurement and
 352 calibration.

353 Measurements of magnetization are performed at a variety of applied
 354 magnetic fields and temperature and are typically expressed in terms of the
 355 saturation magnetization M_0 which is the extrapolation to zero applied field
 356 at 0 K[20]. A review of the literature yields many measurements of the
 357 magnetization of iron and nickel. Different approaches can be taken to ob-
 358 tain “consensus” values. One approach taken by H. Danan *et al.*[21] and
 359 deBever *et al.* [3] is to average the values of spontaneous magnetization
 360 $M_0(H = 0, T = 0 \text{ K})$ and then apply a correction to obtain the magnetiza-
 361 tion at room temperature and nonzero applied fields. However, the process of
 362 extrapolation to zero field and temperature is not standardized and different
 363 methods are utilized, making this a poor standard for comparison. Further-
 364 more, since we are looking for magnetization near room temperature this
 365 method introduces error extrapolating down to M_0 and once again correct-
 366 ing back up to room temperature and high fields. Since most measurements
 367 at least include data at or near room temperature and at internal fields at

or close to 10000 Oe (1 T), it makes sense to utilize magnetization measurements taken near room temperature and internal fields of order 10 kOe. Where the available data in the literature were not available at precisely $T = 294^\circ\text{K}$, small corrections were applied to the measurements based upon the formulation given in [12]. In each case the data of magnetization versus internal magnetic field were parameterized using Eqs. 9 and 10 from [12].

Although the “consensus” values present here for magnetization include data from a number of measurements done over a period from 1929-2001, this is not an exhaustive data set by any means. Table 2 lists the publications used in this analysis for iron and nickel. We established the following criteria to decide which data to include:

- Original data was published and publication was available. Some measurements referred to in the literature are not readily available. For example much of Danan’s reported measurements on Ni were never published except in his 1968 review which provides few details of the experiment.
- Data in the publication were available near room temperature and internal field of 10 kOe. We corrected all data in this analysis to $T = 294$ K. Starting with measurements of the magnetization close to these values of temperature and internal field keeps the corrections and extrapolation uncertainty small.
- Enough details were provided to obtain the internal field of the sample either because the data were given versus internal field or the demagnetizing factor could be calculated from information given.
- Data were taken with a high purity sample. With the exception of the NASA study by Behrendt *et al.* for which purity was not stated, all samples used had greater purity than 99.9% to keep the systematic error from this source small. The NASA study was included in spite of the lack of information on sample purity because they claimed measurement error of $\pm 0.2\%$ and they were only the second data set we found with measurements in the high-field (several tesla) region of interest to us and which met the other criteria.
- Systematic errors were sufficiently small to provide useful additional information. For example, Pauthenet [12] has very precise data, but

402 since he uses Danan’s Ni data for absolute calibration, his systematic
 403 error is 0.5%. Therefore, Pauthenet’s data are used for relative correc-
 404 tions of field and temperature, but not in the absolute measurement
 405 average. Aldred [22] also has a precise data set, but calibrates his data
 406 using the “known magnetization of nickel” which is exactly what this
 407 analysis is seeking to determine. For this reason, we also did not retain
 408 Aldred’s data.

Table 2: Publications used in obtaining consensus value for magnetization near room temperature at high fields.

Publication	Year	T ($^{\circ}K$)	Comment
Weiss and Forrer [23]	1929	288	Only Fe data used
R. Sanford <i>et al.</i> (NIST)[24]	1941	298	Data on Fe only
H. Danan [25]	1959	288	Data on Ni and Fe
Arajs and Dunmyre [26]	1967	298	Data on Ni and Fe
Crangle and Goodman [20]	1971	293	Data on Ni and Fe
Behrendt and Hegland (NASA)[27]	1972	298.9	Data on Fe only
R. Shull <i>et al.</i> (NIST)	2000	298	Data on Ni only

409 Fig.3 shows the data for the magnetization of Fe from the published sources
 410 before and after correction to T=294°K. Where data were not given in terms
 411 of internal field H_{int} , they were converted to H_{int} using Eq. 8 using informa-
 412 tion given in the publications to determine the demagnetizing field $4\pi M/\rho$.
 413 The data are approximately linear as expected in the high-field region above
 414 3 kOe. The lower panel of Fig. 3 shows the data after correction to the
 415 standard temperature 294 K. It is striking that the temperature correction
 416 increases the inconsistency between the different data sets. As previously
 417 mentioned, the temperature correction was taken from Pauthenet’s param-
 418 eterization given in Eq 9 in [12] (see Eq. 7) with the coefficients found
 419 empirically to be $a_{3/2} = 307 \times 10^{-6}$, $a_{5/2} = -22.8 \times 10^{-8}$ and $a_{7/2} = 0$. Pau-
 420 thenet evaluates the factor $g\mu_B/k_B$ as 1.378×10^{-4} .² A linear approximation
 421 $\chi(T) = 3.644 \times 10^{-6} + 5.0434 \times 10^{-10}T$ was obtained from a fit to the discrete

²Note that Pauthenet actually gives $g\mu_B/k_B = 1.378$ for Fe in Eq. 9 of [12], but replicating his plots in Figure 1 of [12] requires an extra factor of 10^{-4} .

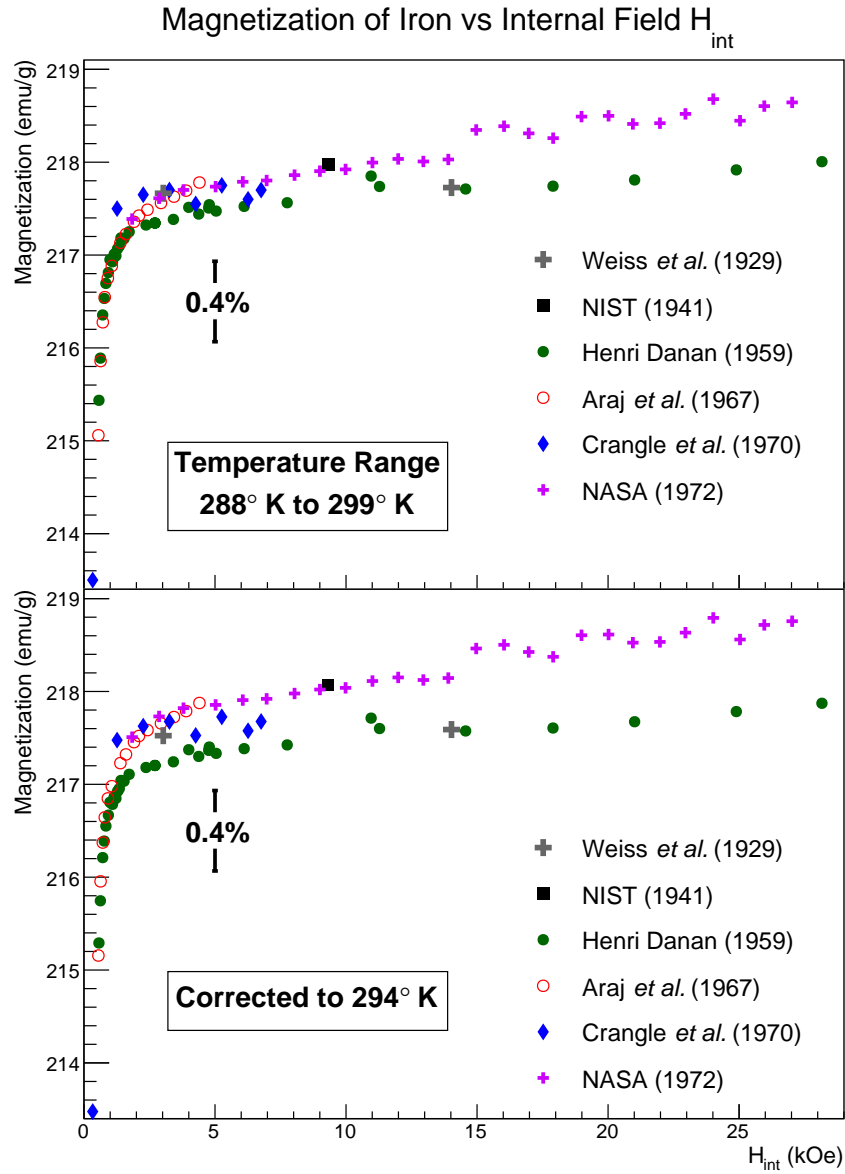


Figure 3: Published magnetization data from various sources for Fe shown versus internal field. The top plot shows data for temperature at which it was taken and the the bottom plot shows the same data corrected to 294°K. Note that zero is suppressed on the vertical axis. Refer to Table 2 for details on the data sets.

422 data points provided in Table 1 of [12] in order to be able to evaluate $\chi(T)$
 423 for any temperature.

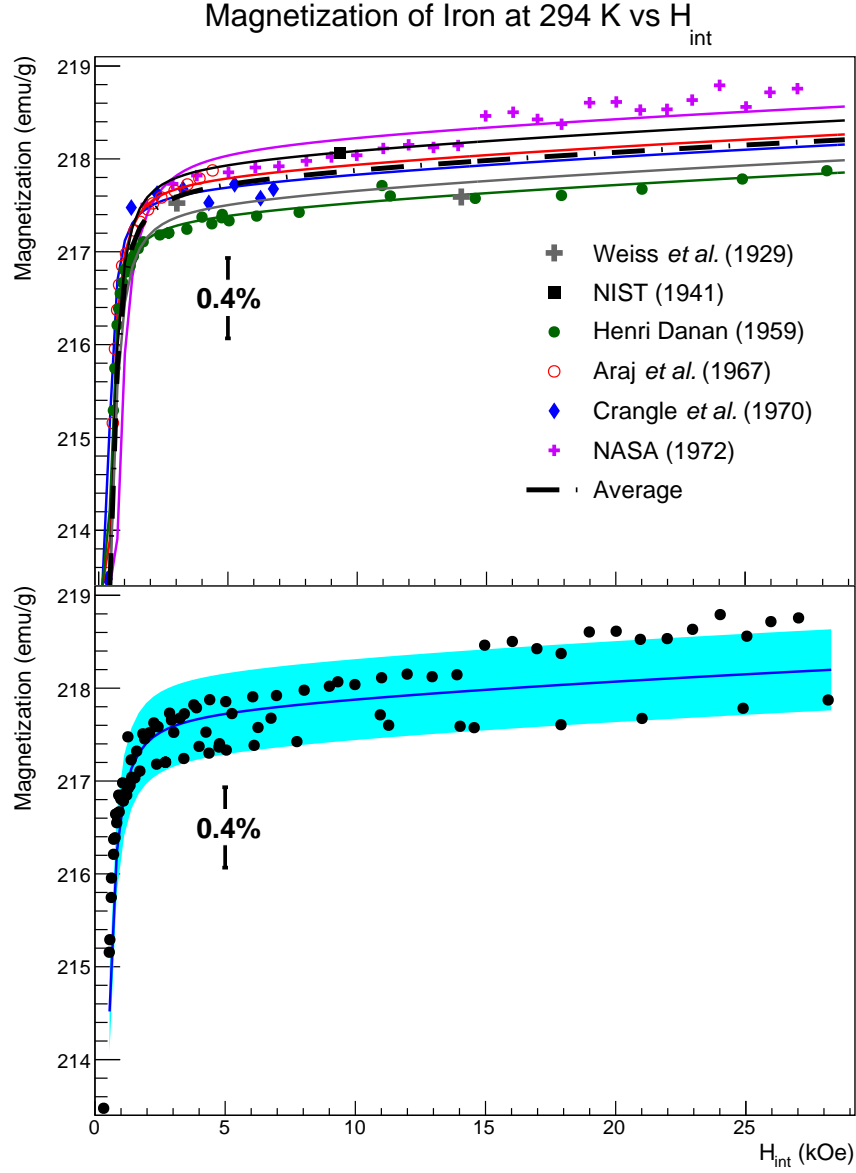


Figure 4: Published magnetization data from various sources for Fe plotted versus internal field corrected to 294°K. Upper plot shows magnetization data fit using a modified form of Eq. 9 from [12]. Each of the six datasets are fit individually and the resulting curve fits averaged (see text for details). Lower plot shows the average parameterization curve for internal fields up to 29 kOe. The error band on the lower plot corresponds to $\pm 0.20\%$ or ~ 0.44 emu/g

424 To get an average parameterization versus internal field, each of the six
 425 temperature-corrected data sets were fit individually using Pauthenet’s pa-
 426 rameterization with $T = 294\text{ K}$ as can be seen in Fig. 4. Pauthenet’s work
 427 was chosen as the high-field reference since he quotes the relative uncertainty
 428 of the data used in his fit to be at the 0.01% level and his parametrization in
 429 the high-field region accurately reproduces the field dependence seen in the
 430 data.

431 An additional term of a/H_{int}^2 was added to Pauthenet’s parameterization
 432 to provide a better fit at low internal field in the approach to saturation.
 433 Pauthenet’s data did not roll off as quickly as the data used here (see Fig.
 434 1 of [12]). The exact curvature in this region is expected to depend on the
 435 composition and purity in addition to stresses and imperfections in the sam-
 436 ple used which will vary from sample to sample. Pauthenet used a high
 437 purity monocrystalline sample aligned along the easy axis to suppress ef-
 438 fects from anisotropy and strains, whereas many of the datasets included
 439 here used polycrystalline samples, providing a plausible explanation of the
 440 discrepancies in this region.

441 Stoner discusses the interpretation of terms proportional to $1/H_{\text{int}}$ as
 442 arising from inclusions (impurities or cavities) in the sample and $1/H_{\text{int}}^2$ as
 443 arising from stresses and imperfections (see discussion around Eqs. 4.18-4.22
 444 in [28] and around Eq. 7 of [29]).

445 For the Fe datasets included here, the term proportional to $1/H_{\text{int}}$ was
 446 not needed, so only a term of the form a/H_{int}^2 was retained. The coefficient a
 447 was constrained to values 0 or below in the fit to maintain consistency with
 448 the physics model. For the data sets with measurements over a range of H_{int}
 449 both M_0 and a were used as fit parameters. In fits for two data of the data
 450 sets (Weiss *et al.* and Sanford *et al.*), only M_0 was allowed to float due to the
 451 limited number of data points and a was fixed to the average from the data
 452 sets where it was allowed to float as a fit parameter. The data for Weiss and
 453 Forrer were not specifically given, but the following linear parameterization
 454 was provided from a fit to data over the range of applied fields from 0.6 to
 455 1.7 T: [23]

$$217.76 \left(1 - \frac{2.6}{H} \right),$$

456 where H is the applied field in oersteds. This parameterization was used to
 457 determine two data points at 0.6 T and 1.7 T which were then fit to determine
 458 M_0 . The data for Sanford (NIST) *et al.* are condensed in the literature to a

single value of H_{int} even though they are composed of multiple values across a range of applied fields not included in the publication.

The average value of M_0 and a from the fits were used to produce the average parameterization curve shown. Over the range of H_{int} from 8 to 28 kOe (about 3 to 5 T applied field for a thin Fe foil magnetized out of plane normal to the surface) the following second degree polynomial accurately follows the average parametrization curve:

$$M_{\text{sat}}^{(\text{Fe})}(H_{\text{int}}, 294 \text{ K}) = 217.628 + 2.7439 \times 10^{-2} H_{\text{int}} - 2.6304 \times 10^{-4} H_{\text{int}}^2, \quad (9)$$

where H_{int} is in units of kOe. This parameterization is shown in Fig.4. A systematic error band of $\pm 0.20\%$ is assigned to account for the spread of the data. The source of this systematic spread across the datasets is not clear.

Using for the magnetic saturation induction ($4\pi M_{\text{sat}}$) of iron 2.157 T and the demagnetizing factor of unity for a thin foil magnetized out of plane, gives an internal field which is 2.157 T less than the applied field near saturation. Thus a uniform external 4 T magnetic field corresponds to an internal field of approximately 1.84 T. Converting Eq. 9 to applied field H in Tesla for the specific case of a thin foil magnetized out of plane gives the following a second order polynomial parameterization accurate over the region of 3-5 T applied field:

$$M_{\text{sat}}^{(\text{Fe})}(\text{emu/g}) = 216.914 + 0.387863 H - 0.026304 H^2. \quad (10)$$

This gives the saturation magnetization per gram for iron at 294°K with an applied field of 4 T as $M_{\text{sat}}^{(\text{Fe})} = 218.04 \pm 0.44 \text{ emu/g}$. This translates into $2.1803 \pm 0.0044 \mu_B/\text{atom}$ which differs slightly from the value of $2.183 \pm 0.002 \mu_B/\text{atom}$ determined by deBever *et al.*[3] partially due to their over-correction for the magnetic field dependence.

A similar analysis of the literature for nickel is shown in Fig. 5. Like for Fe, the Ni data were fit to the Pauthenet parameterization with an additional term of a/H_{int}^2 . Each of the four data sets were fit independently in M_0 and a with a being constrained to be 0 or less as before. The only exception to this parameterization was the Crangle data set where a was fixed at 0 since there were no low field data to guide the fit. The fits are shown in Fig. 6. The “Average” parameterization curve was formed using the average M_0 and a from the fits. This average parameterization along with a proposed systematic error band of $\pm 0.2\%$ or 0.11 emu/g is shown in Fig.6. Using for the magnetic saturation induction of nickel 0.6179 T and the demagnetization

492 factor of unity for a thin foil magnetized out of plane, makes the internal field
 493 0.6179 T less than the applied field near saturation. Thus a uniform external
 494 2 T magnetic field corresponds to an internal field of approximately 1.38 T.
 495 Over the range of H_{int} from 6 to 20 kOe (approximately 1.2 to 2.6 T applied
 496 field for a thin Ni foil magnetized out of plane normal to the surface) the
 497 following polynomial precisely follows the fit parameterization curve:

$$M_{\text{sat}}^{(\text{Ni})}(\text{emu/g}) = 55.063 + 1.5718 \times 10^{-2} H_{\text{int}} - 1.9678 \times 10^{-4} H_{\text{int}}^2, \quad (11)$$

498 with H_{int} in units of kOe. Converting Eq. 11 to applied field H in Tesla for
 499 the specific case of a thin Ni foil magnetized out of plane:

$$M_{\text{sat}}^{(\text{Ni})}(\text{emu/g}) = 54.959 + 0.181495 H - 0.019678 H^2. \quad (12)$$

500 This gives the magnetization per gram for iron at 294°K with an applied
 501 field of 2 T as $M_{\text{sat}}^{(\text{Ni})} = 55.24 \pm 0.11$ emu/g. This translates into $0.5806 \pm$
 502 $0.0012 \mu_B/\text{atom}$

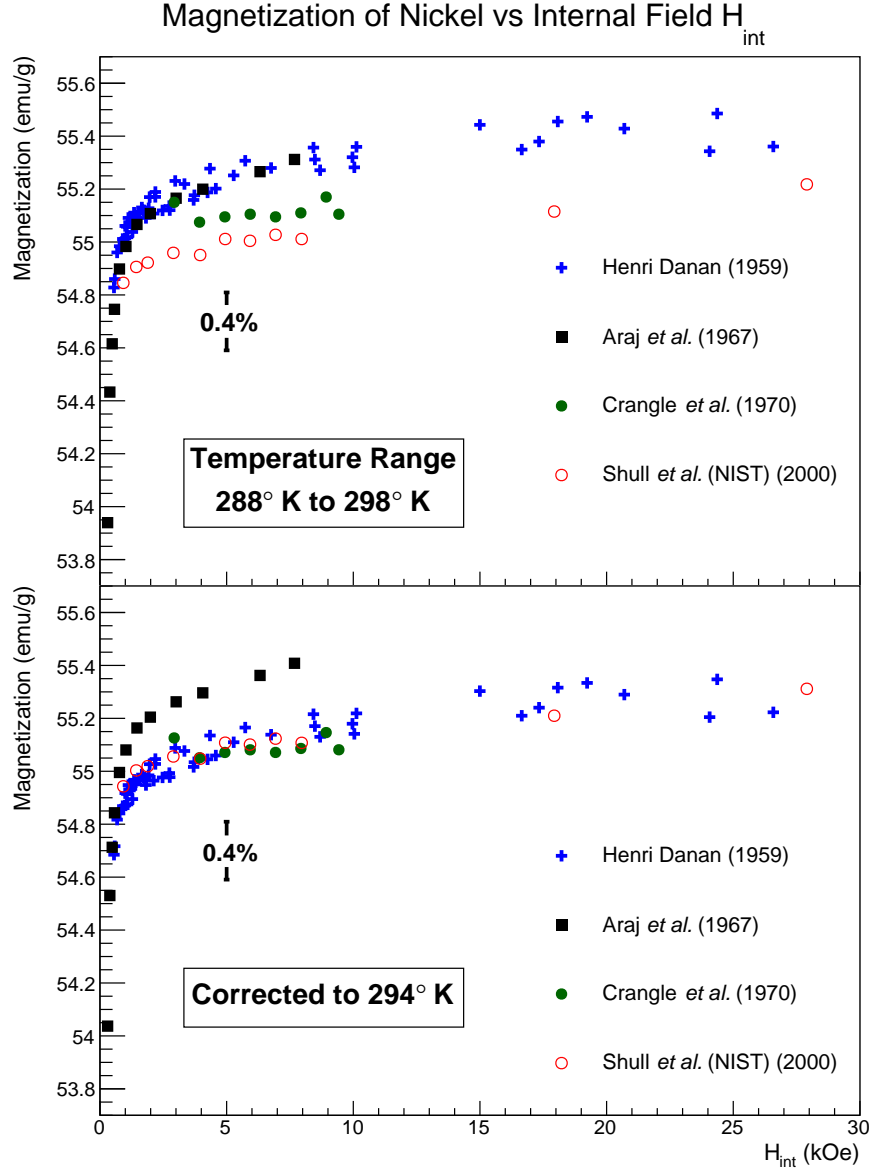


Figure 5: Published magnetization data from various sources for Ni shown versus internal field. The top plot shows data for temperature at which it was taken and the bottom plot shows the same data corrected to 294°K. There is good agreement in the data with the clear exception of that from Aaraj *et al.* which are systematically higher by $\sim 0.5\%$. The reason for this discrepancy is not clear. Their publication claims $\pm 0.2\%$ accuracy for saturation magnetization which cannot explain the full difference.

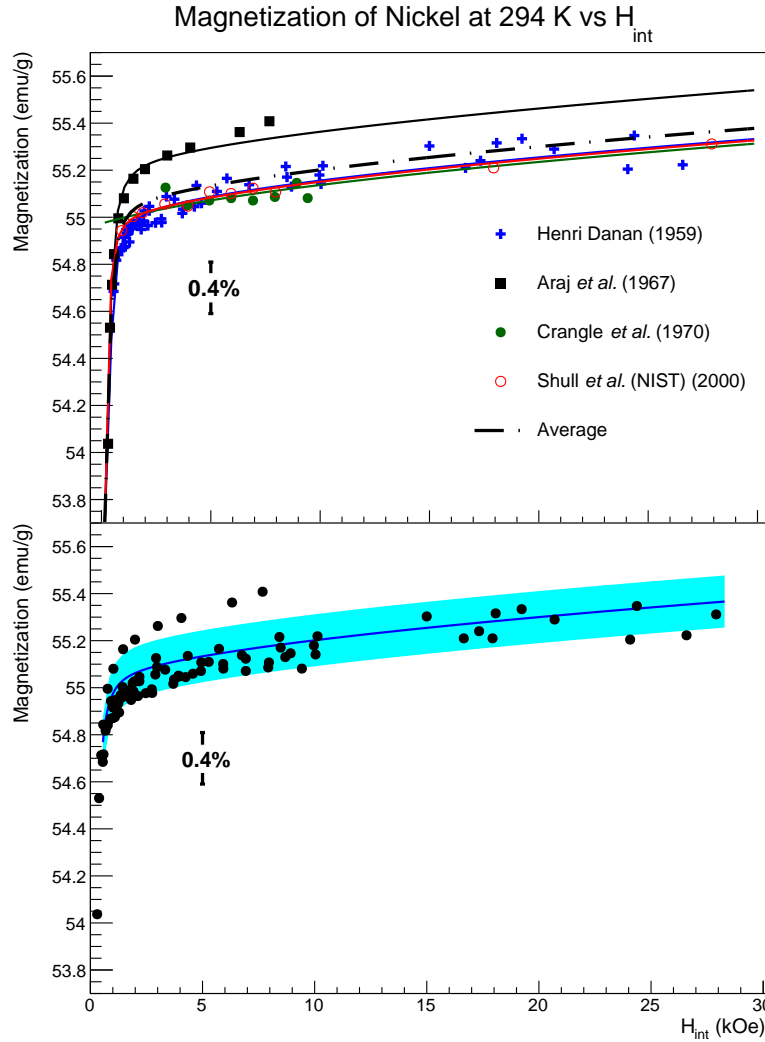


Figure 6: (Top) Published magnetization data from various sources for Ni plotted versus internal field corrected to 294°K and shown with proposed parametrization curve for internal fields up to 20 kOe (2 T). (Bottom) The “Average” curve from the upper plot with a $\pm 0.20\%$ (0.11 emu/g) error band. For a thin nickel foil magnetized out of plane (normal to the surface) close to saturation, the difference between the internal and applied field is about 0.6 T so 2 T external field corresponds to 1.4 T internal field.

503 2.1.4. *Magnetocrystalline anisotropy*

504 As previously discussed in section 2.1.2, the crystal structure of ferromag-
 505 netic elements creates axes along which it is easier or harder to magnetize the
 506 material. The origin of this anisotropy is primarily from the spin-orbit cou-
 507 pling. The spin-spin coupling works to align adjacent spins in either parallel
 508 or anti-parallel orientations but does not couple to the crystal lattice. The
 509 spin-spin coupling can be rotated relatively easily with external magnetic
 510 fields. Conversely, the orbital magnetic moments are strongly coupled to the
 511 crystal lattice such that even very strong magnetic fields do not easily rotate
 512 them. The coupling between the spin and orbital motion of each electron
 513 tends to align the spins of the electrons along the crystal lattice such that
 514 there is an additional energy associated with rotating the spins away from
 515 what is termed the “easy axis” of the crystal. This coupling is also relatively
 516 weak with fields of a few hundred oersteds being sufficient to overcome it.
 517 For a more detailed discussion refer to *An Introduction to Magnetic Materials*
 518 by Cullity and Graham section 7.4[30].

519 Iron and nickel (iron is body-centered cubic and nickel is face-centered
 520 cubic) have hard, medium and easy magnetization axes due to their crys-
 521 tal lattice structure. Magnetization along any axis other than the easy axis
 522 requires a larger applied magnetic field due to the anisotropy energy. The
 523 plots in Fig. 7 show typical magnetization curves for iron and nickel along
 524 each of their magnetocrystalline axes. It is important to note that each of
 525 the magnetization curves in Fig. 7 appears to approach the same saturation
 526 magnetization. Pauthenet measured the saturation magnetization with pre-
 527 cision along the different crystallographic axes for Ni and Fe and concluded
 528 that the saturation magnetization is the same to within 0.01% at an internal
 529 field of 10 kOe or greater[15].

530 2.1.5. *Discussion of cobalt as a potential target material*

531 Two key features of cobalt make it unfit as a precision target material.
 532 First, the crystal structure of cobalt (mainly close-packed hexagonal at room
 533 temperature) creates a greater magnetocrystalline anisotropy than it does for
 534 the other two ferromagnetic elements. Pauthenet measured the difference in
 535 saturation magnetization along the different axes to be at the 0.5% level
 536 in his careful study of magnetization versus field[15]. In a polycrystalline
 537 sample such as a foil that might be utilized in the Møller polarimeter, it is
 538 not apparent how to determine the saturation magnetization.

539 Second, the crystal structure of cobalt changes from primarily close-

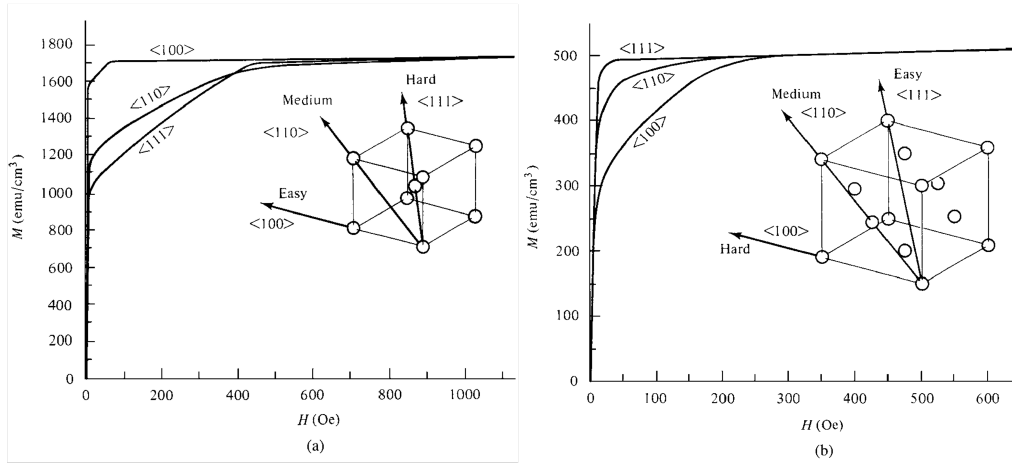


Figure 7: Magnetization curves for single crystals of Fe (a) and Ni (b) demonstrating the relative difficulty of magnetizing the crystals along different directions. (Figure adapted from [30].)

540 packed hexagonal below 690°K to face-centered cubic above this temperature.
 541 Near room temperature, a mixture of the two crystal structures generally of
 542 which the fractional composition varies from sample to sample producing a
 543 large uncertainty in the saturation magnetization for this material[31]. For
 544 these reasons, we have discarded cobalt as a candidate precision target ma-
 545 terial.

2.1.6. Target heating and temperature corrections

The magnetization of Fe and Ni is found for room temperature; however, there is a relatively large temperature-dependent correction ($\sim 1.5\%$ from liquid helium to room temperature for Fe) to the saturation magnetization as discussed in section 2.1.1. We now discuss the temperature corrections to the target magnetization for temperatures above 294 °K.

When the electron beam is on target during a Møller polarimetry measurement, energy deposition causes the foil to heat up by a few degrees under usual conditions. Since there is a slight temperature dependence to the magnetization a correction will have to be applied. The further from the Curie temperature of the material, the smaller the correction will be. Therefore, we can expect the beam heating correction for Ni to be fractionally larger than that of Fe (see Table 1).

In the absence of a direct way of determining the temperature of the foil at the beam spot during operation or of monitoring the relative magnetization *in situ*, an estimate of the temperature increase must be made. This section provides a calculation of the foil heating from the electron beam under a set of assumptions.

The thin foil circular disks used in the Møller polarimeter are a few microns thick (see Fig. 8). The electron beam flux profile is approximately Gaussian with a typical 1σ radius of 100 μm . At Jefferson Lab, the beam radius is measured using Superharps which determine the beam profile by moving thin wires through the beam and measuring the current on the wire as a function of position. These measurements yield separate 1σ radii for the x and y directions. Since this analysis assumes a circular beam distribution, the geometric mean of the 1σ x and y radii can be used: $r_b = \sqrt{\sigma_x \sigma_y}$.

The beam is approximately centered on the Møller target and has a natural helicity-correlated jitter of a few tens of microns. We calculate the approximate foil temperature change based on a few reasonable assumptions. We assume the beam introduces a heat load that is approximately a circular Gaussian distribution centered on the foil disk and that radiative black-body

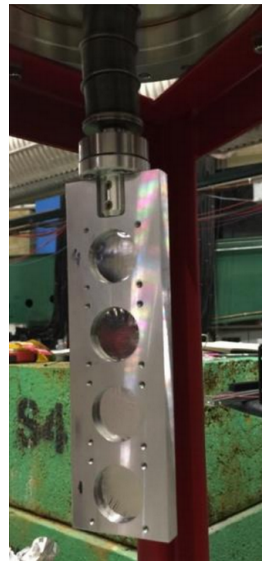


Figure 8: Target ladder with four thin iron foil disks. The support structure is aluminum.

cooling is negligible. We also assume that the aluminum frame constitutes an approximately infinite heat sink i.e. the temperature of the aluminum frame remains at or near room temperature, and that the foils are 0.5 inch in diameter and in perfect thermal contact with the aluminum frame along their edges.

The heat equation for this situation with only radial dependence and in the steady state is given as

$$\kappa \nabla^2 T = -\rho \alpha B_{flux}, \quad (13)$$

which reduces to

$$\frac{\partial}{\partial r} \left(r \frac{\partial T}{\partial r} \right) = -\frac{\rho \alpha}{\kappa} r B_{flux}, \quad (14)$$

where κ is the temperature dependent thermal conductivity of Fe; $\rho = 7.874 \text{ g/cm}^3$ is the density of Fe; α is the collision stopping power for electrons in Fe, which is a function of electron energy; and $B_{flux} = \frac{d^3 N_e}{ds dt}$ is the flux density of the beam in $e^-/(\text{cm}^2 \text{ s})$. This equation can be easily solved numerically with a Gaussian beam profile B_{flux} proportional to $e^{-r^2/2r_b^2}$, where r_b is the 1σ radius of the beam. The solution is shown in Fig. 9 with a $1 \mu\text{A}$ beam heat load with a typical spot size of $r_b = 100 \mu\text{m}$. Fig. 10 shows the dependence of the average temperature rise on the beam spot size for otherwise similar parameters. Using these data we obtained a temperature rise of $12.14^\circ\text{C}/\mu\text{A}$ for Fe as shown in Fig. 9. A similar temperature rise of $12.35^\circ\text{C}/\mu\text{A}$ was found for Ni foil. A COMSOL simulation of heating for Ni and Fe foils under similar assumptions was found to agree well with the temperature rise calculations detailed here.

The temperature dependence of magnetization for iron and nickel from [12, 15] yields the sensitivity shown in Fig. 11. The model was evaluated for applied fields of 2 T for nickel and 4 T for iron. A linear fit to the region of interest for heating from an electron beam between 0.5 and $1.5 \mu\text{A}$ yields slopes of $-0.025 \text{ (emu/g/}^\circ\text{C)}$ for Ni and $-0.024 \text{ (emu/g/}^\circ\text{C)}$ for Fe. A conservative uncertainty of 30% is sufficient to cover both the uncertainties from the calculation of temperature increase and the magnetization versus temperature correction slope, yielding an uncertainty in the magnetization of $\pm 0.09 \text{ (emu/g/}\mu\text{A)}$ for both Ni and Fe.

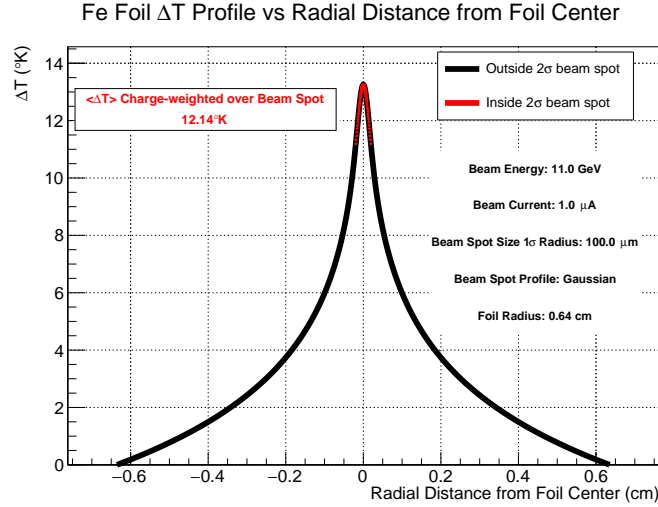


Figure 9: Foil temperature distribution in a 0.5 inch diameter foil under a 1 μA beam load. The electron beam is assumed to have a Gaussian distribution with a beam current and energy, foil radius and 1σ beam radius given in the plot. The red tip of the distribution is the part of the foil inside the 2σ beam spot. The average temperature rise weighted by the beam distribution over the beam spot is also shown. The ROOT macro for making this plot is called “FeFoilHeating.C” and is available at the following Git repository: <https://github.com/jonesdc76/MollerPolarimetry/blob/master/TargetPolarization/>

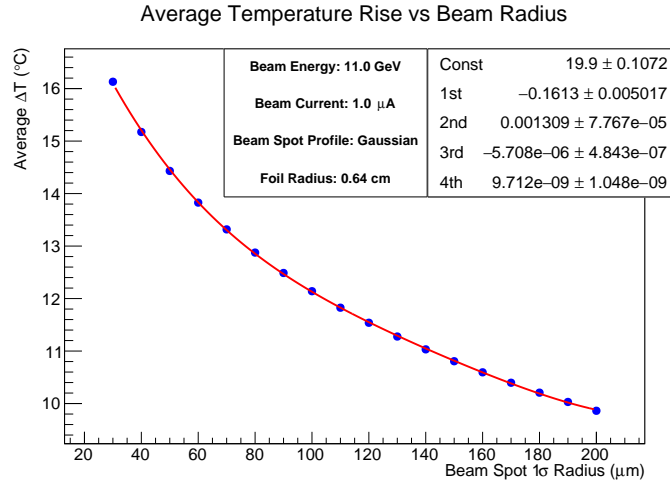


Figure 10: Average foil temperature increase (weighted by the beam charge distribution) shown versus beam spot size radius for the parameters shown. The data are fit to a 4th degree polynomial with the fit parameters shown.

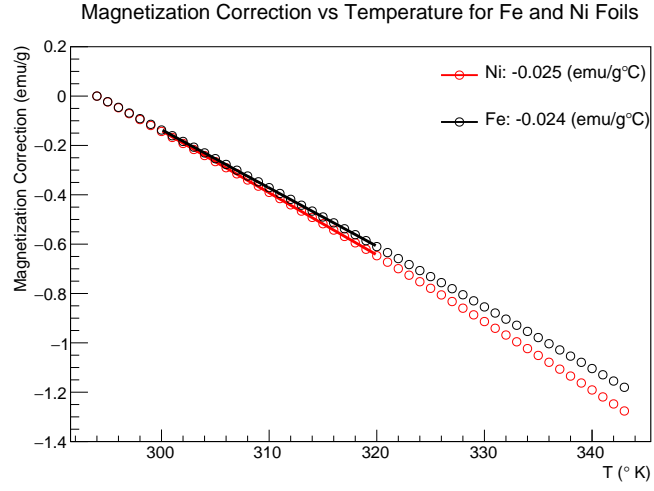


Figure 11: Temperature correction as a function of temperature above room temperature (assumed to be 294 K) for nickel and iron using the model in [12, 15]. The model was evaluated for an applied field of 2 T for nickel and 4 T for iron. The fits are over the temperature range 300 to 320 °K.

2.1.7. Effect of impurities

We next consider the effect of impurities on the measured magnetization. The experiments whose data are used in this analysis (with the possible exception of the measurement at NASA by Behrendt *et al.*) utilized highly pure Fe and Ni samples. Table 3 lists the level of impurities in the samples used in the various experiments whose data are used in this analysis. Although Weiss and Forrer [23] do not give a numerical value for the level of impurities they assure us that there were no impurities at a measurable level. They used this highly pure sample for the most precise results and many samples of less pure iron for less accurate studies. To set the scale, their less pure sample had a total of 0.22% impurities with 0.09% of that being carbon. Although the NASA measurement by Behrendt *et al.* does not list a purity level for the sample, we retain this measurement in spite of this uncertainty since it is only the second data set we found with precision measurements in the high field region (4 T applied fields) where we are typically running. An appropriately large systematic error is assigned in the end to account for this uncertainty.

Addition of non-ferromagnetic impurities typically decreases the magnetization (see for example [35, 36, 24]). Sanford *et al.* corrected for the effect of $\sim 0.01\%$ impurities which yielded a correction at the $\sim 0.02\%$ level[24]. Ahern *et al.* also found that adding copper to nickel reduced the magnetization by about 2% for every 1% of the nickel replaced by copper. If we set the uncertainty from impurities at twice the fractional level of impurities, the largest error (0.12%) comes from the ARAJS and Dunmyre data on iron. Given the purity of the Fe and Ni samples used, we assign no additional systematic error beyond that already determined from the spread in the data. We will revisit the effects of impurities once again in the determination of the spin component of the magnetization.

Another source of impurities generally not accounted for in assays is the surface oxidation. Iron oxides such as Fe_3O_4 , have a much smaller magnetization than pure Fe. Alex Gray's group at Temple University took XMCD measurements for us at the Advanced Light Source on a pure Fe foil which we provided from our Møller target materials. These measurements, which probe the material surface to a depth of a few nanometers, showed clear evidence of surface oxidation in spite of their highly specular appearance. This suggests that foils nearing micron level thickness could have surface contamination from oxides at the 0.1% level. We expect that using clean foils with

Table 3: Level of impurities from the various measurements used in this analysis. Note that Danan used the same Fe sample measured by Weiss and Forrer. Crangle and Goodman used two samples for Fe and two for Ni of differing purities.

Experiment	Element	Impurity Fraction
Weiss and Forrer [23]	Fe	“No detectable impurities”
R. Sanford <i>et al.</i> (NIST)[24]	Fe	<0.01%
H. Danan [25, 21]	Fe	Same as Weiss and Forrer
Arajs and Dunmyre [32][26]	Fe	~600 ppm
Crangle and Goodman [20]	Fe	0.06% and 0.006%
Behrendt and Hegland (NASA)[27]	Fe	Not given
H. Danan [25, 21]	Ni	0.01%
Arajs and Dunmyre [33, 34, 26]	Ni	~30 ppm
Crangle and Goodman [20]	Ni	0.05% and 0.005%
R. Shull <i>et al.</i> (NIST)	Ni	10 ppm

no surface oxidation apparent to the naked eye and with a thickness of 10 μm will render this source of uncertainty negligible at the $\ll 0.1\%$ level.

2.1.8. Nuclear contribution to the magnetic moment

Discussion of the nuclear contribution to the magnetic moment appears to be absent from the literature on magnetization measurements. This is most likely due to the suppression of the nuclear magneton relative to the Bohr magneton by the electron to proton mass ratio ($\mu_B/\mu_N = m_p/m_e$), a factor of about 1/2000. However, in the determination of target polarization for the Møller polarimeter, effects at the 0.1% level require consideration. In the nucleus spins are paired in such a way that all even-even nuclei have zero spin. Fortunately, the isotopic distribution of iron (26 protons) is such that 97.9% of natural iron is from even-even isotopes. The single even-odd naturally occurring isotope ^{57}Fe has a negligible nuclear spin of $0.09\mu_N$ [37]. For nickel (28 protons) the situation is also favorable with natural nickel being composed of 98.9% even-even isotopes. This gives us another two orders of magnitude suppression and renders the nuclear spin contribution completely negligible. However, for cobalt (27 protons), the only stable isotope has a nuclear spin of $4.63\mu_N$, potentially creating errors at the 0.2% level and adding another reason not to use Co foil.

669 *2.2. Determination of g' and the spin component of magnetization*

670 Magnetization arises from a combination of spin and orbital contribu-
671 tions. In ferromagnetic materials, the orbital component is suppressed or
672 “quenched” compared to the spin. To find the spin polarization of the target
673 foils we must determine the spin fraction of the magnetization. The spin
674 component of the magnetization can be determined from measurements of
675 g' , the total g-factor for atomic electrons which can be obtained from magne-
676 tomechanical experiments utilizing the Einstein-de Haas effect or the Barnett
677 effect.³ In general, the g -factor is related to the gyromagnetic ratio γ of a
678 charged body as

$$\gamma = g \frac{e}{2mc} = g \frac{\mu_B}{\hbar}, \quad (15)$$

679 where μ_B is the Bohr magneton.⁴ The electron has two g -factors which we
680 refer to as $g_S \approx 2$ for its spin, and $g_L = 1$ for its orbital motion. For atoms
681 having both orbital and spin angular momentum, g' is a linear combination
682 of g_S and g_L , which is not known *a priori* and must be determined from
683 measurement.

684 In publications from the early to middle 1900s, g_S was assumed to be
685 exactly 2 where we now know it to be (up to a sign) the most precisely
686 measured scientific constant $g_S = 2.00231930436256(35)$. In most cases, this
687 0.1% difference is not consequential, but for the level of precision we are
688 trying to reach, this is not negligible and care must be taken to track down
689 wherever 2 has been substituted for g_S .

690 The relationship of g' to the magnetic moment contribution is often given
691 in the literature following the example of Kittel[42] in the following form:
692 [43, 44]

$$g' = \frac{2(M_S + M_L)}{M_S + 2M_L} = \frac{2M_{\text{tot}}}{M_{\text{tot}} + M_L}, \quad (16)$$

693 where M_{tot} is the total magnetization. M_L and M_S are the components of
694 magnetization arising from orbital and spin magnetic moments respectively.

³The Einstein-de Haas effect (rotation by magnetization) is the rotation of a macroscopic body in a magnetic field when the field is reversed[38, 39]. The Barnett effect (magnetization by rotation) is the converse, the production of a magnetic field by rotation of a macroscopic body[40, 41].

⁴In early publications sometimes the gyromagnetic ratio is given as $\rho = L/M$ the ratio of the angular momentum to the magnetic moment where at other times it is defined in the usual way as the reciprocal $\gamma = 1/\rho = M/L$.

695 This expression immediately leads to the expression of orbital and spin con-
 696 tributions to the magnetic moment as [3]

$$\frac{M_L}{M_{\text{tot}}} = \frac{2 - g'}{g'}, \quad \frac{M_S}{M_{\text{tot}}} = 1 - \frac{M_L}{M_{\text{tot}}}. \quad (17)$$

697 The gyromagnetic ratio, γ is defined as the ratio of the magnetic moment
 698 of a particle or body to its angular momentum. In measurements of g' where
 699 magnetization and angular momentum of macroscopic bodies are directly
 700 measured, the gyromagnetic ratio is determined as

$$\gamma = \frac{M}{J},$$

701 where M and J are the projections of \mathbf{M} and \mathbf{J} along the direction of mag-
 702 netization. We can divide these into their spin and orbital components:

$$M = M_L + M_S, \quad J = J_L + J_S,$$

703 where the subscripts L and S refer to orbital and spin respectively. At
 704 the atomic level the magnetic moment \mathbf{M} is related to the orbital and spin
 705 angular momentum as $\mathbf{M}_S = g_S \mu_B \mathbf{S} / \hbar$ and $\mathbf{M}_L = g_L \mu_B \mathbf{L} / \hbar$, such that a
 706 unit of spin angular momentum yields g_S / g_L more magnetic moment than a
 707 unit of orbital angular momentum. This holds also at the macroscopic level
 708 so that we can write

$$\gamma = g' \frac{\mu_B}{\hbar}, \quad g' = \frac{M_{\text{tot}}}{M_S / g_S + M_L / g_L}. \quad (18)$$

709 To high precision $g_L = 1$ yielding ⁵

$$g' = \frac{M_{\text{tot}}}{M_S / g_S + M_L} = \frac{g_S M_{\text{tot}}}{M_S + g_S M_L}. \quad (19)$$

710 from which we recover Eq. 16 if we substitute $g_S = 2$. Eq. 19 is the exact
 711 form which should be used in this analysis. Furthermore, the exact form of
 712 Eq. 17 is the slightly more complicated

$$\frac{M_L}{M_{\text{tot}}} = \frac{g_S - g'}{g'(g_S - 1)}. \quad (20)$$

⁵There is a small correction to g_L that arises from the finite mass of the nucleus at the order of the ratio of the electron mass to that of the nucleus ($\sim 1 \times 10^{-5}$) [45]. This is two orders of magnitude below the correction considered here of $(g_S - 2) / g_S$ and will be neglected.

713 This gives for the spin component

$$\frac{M_S}{M_{\text{tot}}} = 1 - \frac{M_L}{M_{\text{tot}}} = \frac{g_S(g' - 1)}{g'(g_S - 1)}, \quad (21)$$

714 which decreases the spin contribution to the total magnetization compared
715 to Eq. 17 by 0.11%.

716 2.2.1. g' for Fe

717 The most precise measurements of g' come from measurements of the gyro-
718 magnetic ratio of iron using the Einstein-de Haas effect. These magnetome-
719 chanical experiments are highly elaborate requiring high precision to observe
720 the tiny effects of interest. The Einstein-de Haas experiments are simple in
721 principle: a sample is suspended from a torsion pendulum along the axis of
722 a magnetic field. Upon reversal of the field a small torque on the sample is
723 measured primarily due to reversal of the valence electron spins. In practice,
724 these experiments are highly technical since the torques on the sample from
725 the Earth's magnetic field can be 7-8 orders of magnitude larger than the
726 torques from spin reversal[39]. Elaborate coil setups were utilized to cancel
727 the Earth's field along with any stray magnetic fields in the region and iso-
728 lation systems incorporated to keep the sample free from interference from
729 outside vibrations. The gyromagnetic ratio was then determined from the
730 measured ratio of the angular momentum to the magnetic moment. Similarly
731 complex systems were used in the experiments which measured the Barnett
732 effect. In these experiments a relatively large sample was rotated and the
733 change in magnetic flux measured in a system of pickup coils.

734 A compilation of g' measurements on iron from magnetomechanical ex-
735 periments is shown in Fig. 12. These data were taken from compilations in
736 two papers⁶ by G. Scott in 1962[39] and Meyer and Asch in 1961[43]. For ref-
737 erence, the data included in these compilations comes from [41, 46, 47, 48, 49].
738 The final two measurements done by G. Scott are by far the most precise.
739 It is clear given the fit probability of 0.004 and from discussions of how the

⁶There is two inconsistencies between these references[39, 43]. 1. Table 1 of [43] has Barnett 1941 $\rho e/mc = 1.035$ ($g' = 1.932$) which comes from averaging measurements using the Einstein-de Haas and Barnett effects. Scott seems to only use Barnett's measurements of the Einstein-de Haas effect and quotes Barnett's measurement as $g' = 1.938$. We retain Barnett's average of the two methods. 2. Scott [39] gives Meyer's 1957 value for Fe as $g'=1.932$, whereas Meyer [43] uses 1.929. We use Meyer's value.

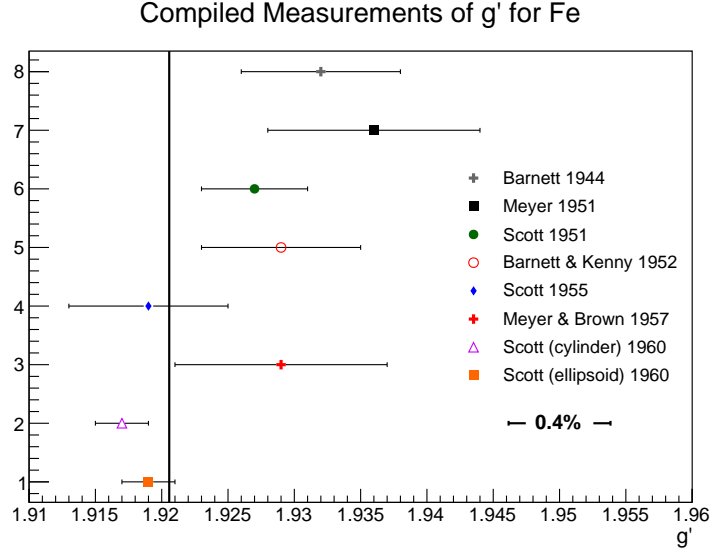


Figure 12: Values of g' for iron as determined by various experiments between 1940 and 1960. The naive constant fit to these data is given by the vertical black line whose value is $g' = 1.9206$.

uncertainties were determined, that the error bars do not in all cases reflect the actual systematic error, which, in at least some of the measurements, is underestimated. The most accurate measurements were made by Scott, who without stated justification, concludes that his most recent measurement of $g' = 1.919 \pm 0.002$ on a prolate ellipsoid sample is the best value to use for iron [49, 39] even though he measured $g' = 1.917 \pm 0.002$ on a cylindrical sample using the same apparatus. It is likely that he regarded the ellipsoid-shaped sample more accurate because this shaped produces It is worth noting that his latest value $g' = 1.919$ appears to be the value taken as standard in the literature (see for example [50, 51]). It not clear what systematics may be at play here (sample purity, shape, porosity, preparation/annealing process).

For the three samples in used in the measurements g' of Fe, the sample purities were as follows:

- Scott cylinder 99.94% with primary impurities O(0.04%), C(0.005%), N(0.004%), S(0.003%) and Ni(0.0015%) [46]
- Scott ellipsoid, 99.89% with primary impurities Ni(0.05%), Si(0.01%), O(0.005%), Co(0.005%) [49]

- Meyer 1957, 99.9% with primary impurities Mn(0.042%), S(0.029%), Si(0.02%) [48]

Scott carefully measured the effect of mixing the ferromagnetic elements Fe, Co and Ni and since their g' values are all within 5% of each other trace amounts of impurities (<1%) from of Ni and Co in Fe will have negligible effect on the value of g' (see Fig 1 of [52]). There is little guidance in the literature for the effect of trace amounts of O, Mn, N, C and S on g' for Fe making it difficult to set the scale for such errors. However, Ladislav Pust *et al.* found very little difference in the related quantity spectroscopic g between pure Fe and that with 3% Si by weight[53]. We will see in the coming paragraphs that the spectroscopic g -factor is inversely related to g' such that if one increases, the other decreases and vice versa.

An error-weighted fit to these data gives a result of 1.9206 ± 0.0012 . However, the χ^2/NDF is 2.41 indicating that systematic errors have been underestimated. Following the example of the Particle Data Group (see Sec. 5.2.2 of [54]), and inflating each of the error bars by $\sqrt{\chi^2/\text{NDF}} = 1.553$ to give a χ^2/NDF of unity (p-value = 0.43) yields an error of 0.0019 or $\pm 0.10\%$.

Related to g' is the spectroscopic g -factor often referred to as g from ferromagnetic resonance (FMR) experiments⁷. FMR works by placing a ferromagnetic sample in a resonant microwave cavity. The cavity is placed in a uniform magnetic field at right angles to the direction of propagation of the microwaves. A microwave source feeds the cavity and a detector monitors the energy coming out of the cavity. When the magnetic field is turned on, the magnetic moments of the atoms will begin to precess around the direction of the applied magnetic field with a frequency that depends on the effective magnetic field H_{eff} and the g -factor of the sample material material as follows:

$$\hbar\omega = g\mu_B H_{\text{eff}} \quad (22)$$

where H_{eff} , the effective magnetic field depends on the applied magnetic field strength as well as the magnetization, shape and relative alignment of the specimen (see [42, 44] for a more detailed explanation). The magnetic field strength is then swept over a range until the resonance condition is met where the precession frequency matches that of the microwave cavity.

⁷For a simple explanation of FMR see <http://www.physik.fu-berlin.de/einrichtungen/ag/ag-kuch/research/techniques/fmr/index.html>

At resonance a drop in power exiting the cavity will be observed due to the energy being absorbed by the sample. Spectroscopic g is determined by measuring the magnetic field which excites this resonance. For a time it was thought that spectroscopic g and g' were the same i.e. that spectroscopic and magnetomechanical experiments were measuring the same g -factor until Kittel (1949)[42] and Van Vleck (1950)[55] independently showed that these are related but not identical quantities. In the case of spectroscopic g , the lattice momentum offsets the intrinsic orbital momentum so that the total angular momentum is approximately equal to the spin contribution[42, 56]. Therefore, spectroscopic g is given by

$$g\left(\frac{e}{2m}\right) = \frac{M_L + M_S}{S},$$

where S is the electron spin. To a good approximation it can be shown that $g = \frac{2M_{\text{tot}}}{M_{\text{tot}} - M_L}$ where g' is given approximately by Eq. 16. Thus, the orbital component increases the magnitude of g and decreases g' . Using these equations we can easily derive what is known as the Kittel-Van Vleck relationship

$$\frac{1}{g} + \frac{1}{g'} = 1. \quad (23)$$

Although this relationship is approximate and should not be considered valid below the $\pm 0.1\%$ level, it has been shown to work quite well in the literature (see for example Fig. 1 of [43]). Therefore, we can utilize spectroscopic measurements of g to further check our value of g' . Figure 13 shows a compilation of measurements of g for iron. A simple error-weighted fit to these data gives a value of $g = 2.086 \pm 0.004$. Using Eq. 23 gives $g' = 1.921$ in precise agreement with the error weight fit to g' from magnetomechanical experiments. While we cannot place the same confidence in this derived value of g' as the direct measurements, it is reassuring that determinations from completely different techniques appear to be consistent.

Recommendation for Fe: In light of these findings we recommend using the value of the simple error-weighted fit with an inflated systematic error to reflect the tension in the world data: $g' = 1.9206 \pm 0.0019$. The 0.0019 error comes from inflating the error reported by the fit by 55.3% which is required to remove the tension in the data and give a χ^2/NDF of 1. The systematic error from impurities is assumed to be included in this uncertainty. This choice places Scott's recommended value of $g' = 1.919 \pm$

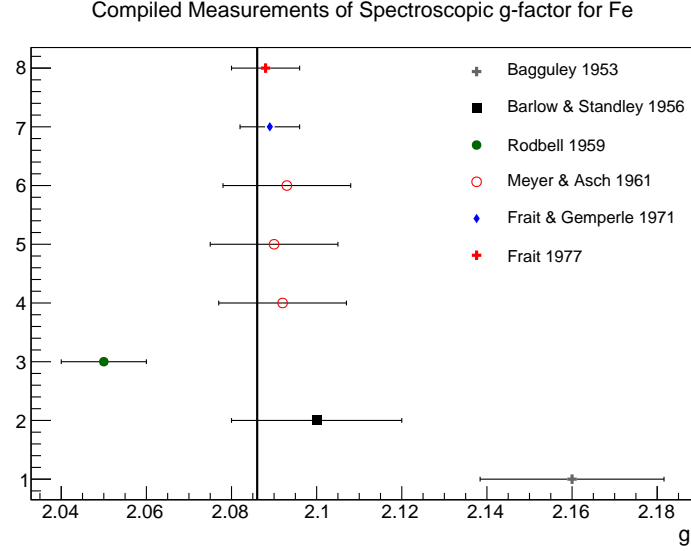


Figure 13: Values of spectroscopic g as determined by various experiments over two decades. The error-weighted fit to these data is given by the vertical black line whose value is $g = 2.086$.

0.002 measured on an ellipsoid Fe sample [39] comfortably within 1σ but his earlier measurement on a cylindrical sample 1.9σ off.

2.2.2. g' for Ni

A number of measurements of g' for nickel were performed by A. J. Meyer *et al.*, G. G. Scott *et al.* and S. Barnett *et al.* during the 1950's. At first there were striking differences in the values found for nickel ranging from 1.83 to >1.99 . Furthermore, the measurements of spectroscopic g from resonance experiments gave a much lower value of g' using the Eq. 23. A couple of systematic errors in the measurement techniques of both Meyer and Scott were pointed out by Brown which brought the data into much better agreement[39]. However, a considerable inconsistency remained between the measurement of Barnett *et al.* and that of Scott and Meyer. Barnett determined $g' \approx 1.91$ compared to the 4% lower $g' \approx 1.84$ found by Meyer and Scott[43, 39]. To investigate the possible reasons for this discrepancy, Meyer measured the Curie temperature and the saturation magnetization of the Ni samples used in each of the measurements. Whereas Scott and Meyer had used nearly pure Ni, Barnett's sample had 1.4% impurities. The presence of these impurities significantly changed the magnetic properties of his Ni

sample such that the Curie temperature was reduced from 360°C for pure Ni to 285°C and the saturation magnetization increased from 58.90 to 71.04 (in units of abamp cm³/g)[39]. Scott concludes that this stark shift in magnetic properties makes Barnett’s measurements “difficult to retain”[39]. However, this discrepancy provides evidence that the presence of certain impurities can have a significant effect on the measurement of g' .

Scott performed a series of four measurements on the same Ni sample in 1952, 1953, 1955 and 1960 and concluded that $g' = 1.835 \pm 0.002$ [39]. Meyer *et al.* also measured g' for different Ni samples in 1957 and 1958 finding 1.852 ± 0.009 and 1.845 ± 0.007 [43]. An error-weighted fit to these values gives $g' = 1.8365 \pm 0.0019$ with a χ^2/NDF of 2.5.

The impurities in the samples used are as follows:

- Scott: 99.82% Ni with main impurities Si(0.1%), Fe(0.032%), Mn(0.030%), and C(0.01%)[57]
- Meyer, 1957: 99.9% Ni with impurities not provided[48]
- Meyer, 1958: 99.99% with negligible impurities[43]

Looking at the impurities in Scott’s sample, we can rule out the effects of Fe and Mn as contributing significantly to a systematic offset using the data in [58, 52]. With carbon impurities at 0.01% this can be considered negligible. Meyer’s analysis of the magnetic properties of the Ni sample used by Scott showed that although the saturation magnetization was changed insignificantly, the Curie temperature decreased by 11°C. Since we were not able to locate data to calibrate the effect Si impurities at 0.1% in Ni, a similar approach to that used for the Fe data will be used here. Inflating the error bars on each of the three data points by 1.581 gives a best fit of $g' = 1.8365 \pm 0.0030$ with a p-value of 0.37.

Once again we can use measurements of the spectroscopic g -factor from magnetic resonance experiments and Eq. 23 as an independent check of our proposed value of g' . Table II. of Meyer and Asch [43] provided a compilation of g -factors measured in magnetic resonance experiments and concluded that for nickel $g = 2.185 \pm 0.010$ which translates into $g' = 1.844 \pm 0.008$ in good agreement with our proposed value.

Recommendation for Ni: in light of these findings we recommend using the value $g' = 1.8365 \pm 0.0030$ for nickel. The value comes from

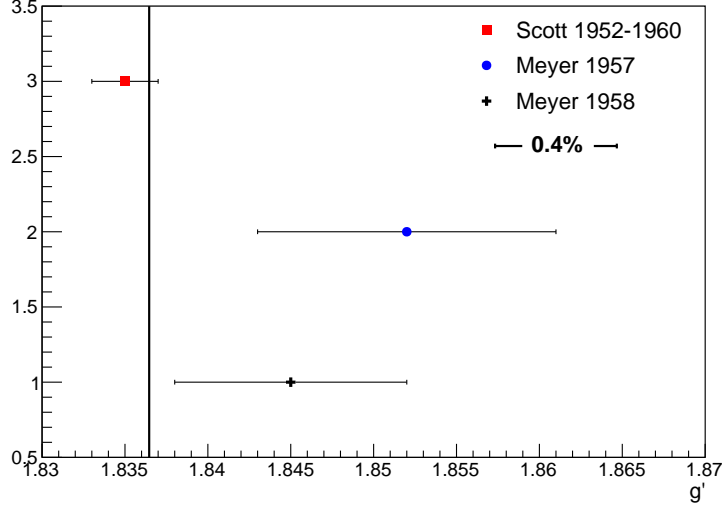


Figure 14: Values of g' for nickel as determined by various experiments between 1950 and 1960. The systematic error on Scott's value as proposed in the text is shown. The error-weighted fit to these data using the proposed error given by the vertical line is $g' = 1.8365 \pm 0.0036$.

an error-weighted fit to Scott's and Meyer's measured values after increasing each of the error bars by 1.581 to accommodate for the underestimated systematic uncertainty.

2.2.3. Temperature dependence of g'

The measurements of g' used in this analysis have all been at room temperature which is not well-defined but is broadly accepted to be near 20°C give or take a few degrees. Although the target foils in the Møller polarimeter will generally be at room temperature, during measurements with a typical 1 μ A of beam on target, the foils will heat up by 10-15 degrees Celsius as we saw in Section 2.1.6. This raises the question of whether or not the room temperature values of g' are sufficiently accurate during measurements at elevated temperatures.

The temperature dependence of saturation magnetization arising from spin waves was discussed in section 2.1.1. If this change in saturation magnetization results in a change of the fraction of magnetization arising from orbital and spin components, this would necessarily imply a change in g' . Conversely, a temperature-independent g' would imply that spin waves pro-

890 proportionately decrease both the orbital and spin components of magnetization.

891 In Kittel's 1949 paper on the relation of g and g' , he discusses the tem-
892 perature dependence of g' and suggests there is not enough data to make
893 conclusions[42]. Since then several measurements have been made of g across
894 a broad temperature range for the ferromagnetic elements and alloys. These
895 experiments, which measure g since it is a technically much easier measure-
896 ment than g' , particularly with changing temperatures, are typically at the
897 1-2% precision level. However, a change in g indicates the inverse change in
898 the g' by Eq. 23. A nice summary of these measurements is found in [59].

899 It is worth noting that in all cases where pure Ni and Fe were measured,
900 the g -factor was always found to be constant within experimental errors,
901 typically at the 1-2% level. However, for alloys, this is not always the case
902 with variations of several percent being observed (see for example [60, 61]).

903 In two cases, extremely accurate measurements were made across a broad
904 temperature range, one for pure Ni and the other for 97% Fe. The first
905 of these was by G. Dewar *et al.* in 1977 on pure nickel foil of 20 μm
906 thickness. They found $g = 2.187 \pm 0.005$ constant over the temperature
907 range 20-364°C[62]. This constitutes a 0.23% test of temperature depen-
908 dence over a range much larger than we care about. The second experi-
909 ment in 1981 by Ladislav Pust and Zdenek Frait measured the g -factor of
910 Fe-3wt%Si in the temperature range from 3.5 to 300 K to be constant at
911 $g = 2.0793 \pm 0.0005$ [63]. The extreme accuracy of their measurement al-
912 lowed them to probe the temperature dependence of g at the 0.02% level and
913 they conclude that there is no evidence of temperature dependence across
914 the temperature range they measured. The plot from their paper showing
915 the measurement of g with temperature is shown in Fig. 15. A summary of
916 the various measurements of g is provided in Table 4.

917 Thus, there is strong evidence that spectroscopic g and by extension g'
918 are, in fact, highly constant for nickel and iron well below their Curie tem-
919 peratures. This implies that the spin-wave correction does not significantly
920 alter the fraction of magnetic moment arising from orbital and spin contribu-
921 tions for these two ferromagnetic elements. We will revisit spin waves in the
922 context of the field-dependence of g' , but we conclude that it is safe to pro-
923 ceed with confidence using the room temperature measurements of g' with
924 negligible error.

Table 4: Results of experiments measuring the spectroscopic g -factor as a function of temperature for various ferromagnetic materials. Without exception all consider the g -factor to be constant within error.

Publication	Year	Material	g -factor	Temp. ($^{\circ}\text{C}$)
Frait <i>et al.</i> [63]	1981	Fe-3wt%Si	2.0793 ± 0.0005	-270 to 27
Haraldson <i>et al.</i> [64]	1981	Ni	2.20 ± 0.02	20 to 358
Gadsden <i>et al.</i> [60]	1978	Ni	2.20	-269 to 20
Dewar <i>et al.</i> [62]	1977	Ni	2.187 ± 0.005	20 to 364
Bastian <i>et al.</i> [65]	1976	Ni-Fe alloys	const. $\pm 1\%$	20 to >300
Rodbell [66]	1964	Ni	2.22 ± 0.03	-140 to 360
Rodbell [67]	1959	Fe	2.05 ± 0.01	-196 to 850
Standley <i>et al.</i> [58]	1955	Ni	2.17 - 2.18	20 to 200
Bagguley <i>et al.</i> [68]	1954	Ni	2.22 ± 0.02	20 to 600
Bloembergen [69]	1950	Ni	2.20 ± 1 - 2%	24 to 358

2.2.4. Magnetic field dependence of g'

In the 1950's while Scott was performing precise measurements of g' , he initially found that g' decreased at very low fields and asymptotically approached a larger constant value at higher fields. He published three papers documenting the low-field behavior of g' for nickel and iron and alloys of the two [70, 57, 71]. In 1960, he found that this low-field behavior was due to a systematic error in his measurement technique[49]. After improving the technique and re-measuring, he concluded that, in fact, g' is independent of applied field for Ni and Fe over the range of fields he was measuring. His setup utilized a solenoid with a total area 78000 cm^2 which he energized with 1-16 mA producing fields as high as 40 gauss. Although these fields were sufficient to induce significant magnetization in the elongated samples, the high currents only induced magnetizations approaching half the level of saturation magnetization. Here we look at evidence to demonstrate that g' remains field-independent in the several tesla applied field region where the Møller polarimeter operates.

FMR measurements of spectroscopic g are taken with the sample at saturation magnetization where the magnetization is well-determined from the literature and the g -factor can be calculated (see Eq. 22). The frequency independence of the g -factor often tested in the literature is simultaneously

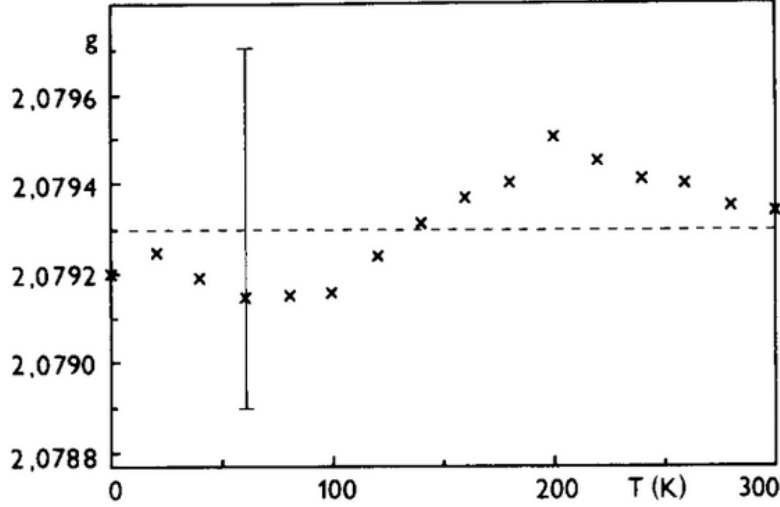


Figure 15: Plot of g -values vs. temperature taken from [63]. The vertical bar denotes the accuracy of these values (± 0.0004).

945 a test of the magnetic field-dependence of g since the frequency is a function
 946 of the effective field, H_{eff} .

947 In 1971, Z. Frait and R. Gemperle measured the g -factor of single iron
 948 crystals across a range of frequencies from 12 to 70 GHz requiring a broad
 949 range of static magnetic fields[72] which roughly corresponds to applied fields
 950 from 0.08 T to 1.6 T (for details on converting between resonance frequency
 951 and applied field see Kittel[73]). They found that $g = 2.089 \pm 0.007$ and that
 952 it is frequency independent over this range within their experimental error
 953 ($\pm 0.33\%$). In 1977, Z. Frait published an FMR measurement of $g = 2.088 \pm$
 954 0.008 for pure polycrystalline iron at three frequencies, 26 GHz (at 0.32 T),
 955 36 GHz (at 0.57 T) and 70 GHz (at 1.53 T)[74]. Once again he concluded that
 956 within experimental error this value is frequency independent, constituting
 957 a high-field test of field dependence on g for iron. Unfortunately, Pust *et al.*
 958 make no mention of frequency-dependence in their $\pm 0.024\%$ measurement
 959 of the g -factor of Fe-3wt%Si even though their results were averages of four
 960 different frequencies, 36 GHz, 70 GHz, 86 GHz and 95 GHz[63].

961 For nickel the data are less precise but point to the same conclusion that
 962 g is field-independent. In 1950 Bloembergen measured the g -factor of nickel
 963 to be 2.23 at 9.05 GHz with a field of 0.116 T and 2.24 at 22.44 GHz with

964 a magnetic field of 0.54 T. These values are equal within the error of the
 965 experiment. In 1959, Rodbell found that for nickel g was constant at the
 966 0.5% level over a range of magnetic fields up to 0.3 T[67]. In 1965, Frait
 967 found that g was independent of frequency for pure nickel at the 2% level
 968 over a range of frequencies from 8.5 GHz to 72 GHz (roughly corresponding
 969 to applied fields of 0.1 T - 2.4 T). He also found that an alloy consisting of
 970 42% Fe and 58% Ni was independent of frequency over the same range at
 971 the 1% level[75]. Finally, as we saw earlier in Section 2.2.3 the value of g'
 972 for nickel derived from high-field measurements of g agrees well within error
 973 with the direct measurements at low field, providing further evidence of the
 974 validity of the asymptotic value of g' for nickel.

975 Although we found no field-dependence of g' for Fe and Ni in the liter-
 976 ature, the evidence is not sufficiently precise to rule out 0.1% level changes
 977 at high field. Given this consideration we chose to place an upper limit on
 978 the field dependence using measurements of high-field susceptibility as we
 979 outline next.

980 Given that g' provides a measure of the fraction of the magnetization
 981 from orbital and spin contributions (see Eq. 20) any field dependence of g or
 982 g' is a signal that the fractional contribution from spin is field-dependent. In
 983 section 2.2.3, we concluded that the spin-wave correction did not significantly
 984 alter g' as evidenced from the temperature independence of g ; however, there
 985 are other field-dependent contributions to magnetization which can be sep-
 986 arated from the spin-wave contribution by either going to the high-field or
 987 low temperature regime where spin-wave contributions are negligible. The
 988 linear increase of magnetization with applied field in the high-field region is
 989 referred to as the high-field susceptibility $\chi_{\text{HF}}(H) = \partial M / \partial H$. χ_{HF} is com-
 990 posed of both orbital and spin contributions[76, 77, 11]. Some attempts have
 991 been made to calculate the relative contributions of the orbital and spin to
 992 the high-field susceptibility[78]. An upper limit on the field dependence of
 993 the spin fraction can be made by assigning the full high-field change in mag-
 994 netization solely to a spin or to an orbital contribution. Tables 5 and 6 list
 995 5 measurements of the high-field susceptibility for Fe and Ni respectively.
 996 The average of the five measurements is 0.0065 emu/(g kOe) for Fe and
 997 0.0025 emu/(g kOe) for Ni. The error is given by the product of χ_{HF} and the
 998 internal field in the foil divided by the saturation magnetization. For Fe (Ni)
 999 foils the field is set to 4 (2) T giving an internal field of 18.4 (13.8) kOe. With
 1000 saturation magnetization for Fe (Ni) of 218 (55.2) emu/g this gives a final
 1001 percent error of 0.055 (0.063)%. We add this additional error in quadrature

with the error in the orbital fraction propagated from the uncertainty in g' .

Table 5: Measurements of χ_{HF} in the high-field and/or low temperature regime for iron. The measurement by Herring *et al.* is almost 3 times larger than the average of the others. The reason for this is not clear, but this measurement was conservatively retained in the average. The “Error” column is the percent contribution to the magnetization at an applied field of 4 T.

Publication	Material	$\chi_{\text{HF}} \left(\frac{\text{emu}}{\text{g kOe}} \right)$	Error %
Herring <i>et al.</i> 1966 [76]	Fe+4%Si	0.0140	0.118
Foner <i>et al.</i> 1966 [79]	Fe	0.0051	0.043
Stoelinga <i>et al.</i> 1966 [77]	Fe	0.0041	0.035
Foner <i>et al.</i> 1969 [11]	Fe	0.0055	0.046
Pauthenet <i>et al.</i> 1982 [12]	Fe	0.0036	0.031
Average		0.0065	0.055

Table 6: Measurements of χ_{HF} in the high-field and/or low temperature regime for nickel. Once again, the measurement by Herring *et al.* is 3 times larger than the average of the others. The “Error” column is the percent contribution to the magnetization at an applied field of 2 T.

Publication	Material	$\chi_{\text{HF}} \left(\frac{\text{emu}}{\text{g kOe}} \right)$	Error %
Herring <i>et al.</i> 1966 [76]	Ni	0.0056	0.141
Foner <i>et al.</i> 1966 [79]	Ni	0.0012	0.031
Stoelinga <i>et al.</i> 1966 [77]	Ni	0.0023	0.057
Foner <i>et al.</i> 1969 [11]	Ni	0.0019	0.048
Pauthenet <i>et al.</i> 1982 [12]	Ni	0.0016	0.040
Average		0.0025	0.063

3. Calculation of Target Polarization

We are now in a position to calculate the final target polarization and the uncertainty on the value. Tables 7 and 8 provide the data for Fe and Ni respectively. The values for magnetization and polarization are calculated for applied magnetic fields of 4 T and 2 T for Fe and Ni foils respectively. In the calculation of target polarization by deBever *et al.* [3], the spin of an electron is assumed to be $1 \mu_B$. This is an approximation valid in the limit that $g_S = 2$ and introduces an error at the 0.1% level. The calculation is as follows:

$$\hat{\mu} = g_S \frac{e}{2m_e} \hat{S}_z = g_S \mu_B \frac{1}{\hbar} \hat{S}_z.$$

Substituting the eigenvalues of spin $S_z = \pm \hbar/2$ gives

$$\mu = \pm \frac{g_S}{2} \mu_B.$$

Thus the spin of an electron is approximately $1.00116 \mu_B$.

Temperature corrections due to target heating are calculated for a $1 \mu\text{A}$ beam load. To first order, increasing the beam load linearly increases the temperature correction whereas increasing target thickness leaves the temperature unchanged. This insensitivity of temperature to thickness is due to the assumption of a good thermal contact with an infinite heat sink at the foil edge. Under these assumptions, the increased conduction of the thicker

1020 foil offsets the additional heat load. Therefore, increasing foil thickness is
the better choice for increasing scattering rates.

Table 7: Summary of values and errors involved in calculating the target polarization for Fe foils.

Quantity	T=294 K	T=306 K	Unit
Saturation magnetization M_s	218.04(44)	217.76(44)	emu/g
Saturation magnetization M_s	2.1803(44)	2.1774(44)	μ_B /atom
g'	1.9206(19)	1.9206(19)	—
Orbital fraction: $\frac{M_L}{M_{\text{tot}}} = \frac{g_S - g'}{g'(g_S - 1)}$	0.0425(10)	0.0425(10)	—
Spin component: $M_S \left(1 - \frac{M_L}{M_{\text{tot}}}\right)$	2.0877(47)	2.0850(48)	μ_B /atom
Average electron magnetization	0.08030(18)	0.08019(19)	μ_B
Average electron polarization	0.08020(18)	0.08010(19)	—

1021

Table 8: Summary of values and errors involved in calculating the target polarization for Ni foils.

Quantity	T=294 K	T=306 K	Unit
Saturation magnetization M_s	55.24(11)	54.94(14)	emu/g
Saturation magnetization M_s	0.5806(12)	0.5774(15)	μ_B /atom
g'	1.8365(30)	1.8365(30)	—
Orbital fraction: $\frac{M_L}{M_{\text{tot}}} = \frac{g_S - g'}{g'(g_S - 1)}$	0.0901(18)	0.0901(18)	—
Spin component: $M_S \left(1 - \frac{M_L}{M_{\text{tot}}}\right)$	0.5283(15)	0.5254(17)	μ_B /atom
Average electron magnetization	0.018867(53)	0.018764(61)	μ_B
Average electron polarization	0.018845(53)	0.018742(61)	—

1022 Thus we have demonstrated that the saturation polarization of an Fe
1023 target can be determined to $\pm 0.23\%$ under a 1 μA beam load, typical for
1024 Hall A at Jefferson Lab. For the same conditions the polarization for a Ni
1025 target can be determined to $\pm 0.33\%$. However, it is important to verify
1026 that the target truly is saturated at the magnetic field settings for a given
1027 experiment. Further discussion of this topic including sensitivity to target
1028 alignment and flatness are a topic for an additional publication.

A total of $\pm 0.25\%$ is currently allotted in our proposed uncertainty budget for target polarization for the MOLLER experiment, implying that we must demonstrate that we are within 0.1% of saturation for an iron target. Although Ni polarization uncertainty is significantly higher than Fe, a significant contribution that can be greatly reduced comes from the heating correction. The heating correction for Ni is much larger than for Fe due to its low Curie temperature. Reducing the current from 1 to 0.3 μA for a Ni foil reduces the overall systematic error from $\pm 0.33\%$ to $\pm 0.28\%$. Thus, a single precision, low current measurement on a Ni foil could be of value for crosschecking the systematic error on the polarization for Fe.

4. Concluding Discussion

The polarization of a saturated ferromagnetic target has been calculated for both nickel and iron foils. With the stringent demands of the proposed MOLLER experiment, it seemed wise to revisit the study of Fe target polarization by deBever *et al.*[3]. A different approach was taken than that in [3] where instead of using the saturation magnetization value at 0 K and then correcting back to room temperature, measured values of magnetization were taken at or near room temperature. A small error was found in the magnetic field correction in equation (3) of [3] where the applied magnetic field was used instead of the internal magnetic field, introducing a small error of about 0.1%. Using the approximation $g_S = 2$ also introduced further errors of order 0.1% in [3].

Using measurements of magnetization and g' we calculate the saturation target polarization for Fe foils at room temperature with 4 T fields applied normal to the foil to be 0.08020 ± 0.00018 . For Ni foils under a 2 T applied field, the saturation polarization is 0.018845 ± 0.000053 . We are optimistic that utilizing an Fe foil target will allow us to reach our uncertainty goal of $\pm 0.25\%$ for target polarization including all uncertainties.

Recent evidence from measurement in Hall A revealed our sensitivity to wrinkles in the foil and raised questions about how well our foils were aligned normal to the holding field. Deviations of the foil surface from normality make it more difficult to reach saturation which is the only place where polarization is known with high accuracy. Further studies will be needed and are ongoing to determine the level of foil flatness required and our sensitivity to foil alignment angle. These are topics of discussion for a future publication.

References

- [1] The MOLLER Collaboration, The MOLLER experiment: An ultra-precise measurement of the weak mixing angle using Møller scattering (2014). [arXiv:1411.4088](#).
- [2] The SoLID collaboration, SoLID (Solenoidal Large Intensity Device) updated preliminary conceptual design report.
URL <https://hallaweb.jlab.org/12GeV/SoLID/files/solid-precdr-Nov2019.pdf>
- [3] L. de Bever, J. Jourdan, M. Loppacher, S. Robinson, I. Sick, J. Zhao, A target for precise Møller polarimetry, Nuclear Instruments and Methods in Physics Research Section A: Accelerators, Spectrometers, Detectors and Associated Equipment 400 (2) (1997) 379 – 386. doi:[http://dx.doi.org/10.1016/S0168-9002\(97\)00961-3](http://dx.doi.org/10.1016/S0168-9002(97)00961-3).
URL <http://www.sciencedirect.com/science/article/pii/S0168900297009613>
- [4] M. Swartz, H. Band, F. Decker, P. Emma, M. Fero, R. Frey, R. King, A. Lath, T. Limberg, R. Prepost, P. Rowson, B. Schumm, M. Woods, M. Zolotorev, Observation of target electron momentum effects in single-arm mller polarimetry, Nuclear Instruments and Methods in Physics Research Section A: Accelerators, Spectrometers, Detectors and Associated Equipment 363 (3) (1995) 526–537. doi:[https://doi.org/10.1016/0168-9002\(95\)00384-3](https://doi.org/10.1016/0168-9002(95)00384-3).
URL <https://www.sciencedirect.com/science/article/pii/0168900295003843>
- [5] D. Adhikari, *et. al.*, Accurate determination of the neutron skin thickness of ^{208}Pb through parity-violation in electron scattering, Phys. Rev. Lett. 126 (2021) 172502. doi:[10.1103/PhysRevLett.126.172502](https://doi.org/10.1103/PhysRevLett.126.172502).
URL <https://link.aps.org/doi/10.1103/PhysRevLett.126.172502>
- [6] Y. Kraftmakher, Spontaneous magnetization of ferromagnets, American Journal of Physics 73 (12) (2005) 1191–1194. [arXiv:https://doi.org/10.1119/1.1994857](#), doi:[10.1119/1.1994857](https://doi.org/10.1119/1.1994857).
URL <https://doi.org/10.1119/1.1994857>

- 1097 [7] C. Kittel, Physical theory of ferromagnetic domains, Rev. Mod. Phys.
1098 21 (1949) 541–583. doi:10.1103/RevModPhys.21.541.
1099 URL <https://link.aps.org/doi/10.1103/RevModPhys.21.541>
- 1100 [8] F. Bloch, Zur theorie des ferromagnetismus, Zeitschrift für Physik 61 (3)
1101 (1930) 206–219. doi:10.1007/BF01339661.
1102 URL <http://dx.doi.org/10.1007/BF01339661>
- 1103 [9] C. Herring, C. Kittel, On the theory of spin waves in ferromagnetic
1104 media, Phys. Rev. 81 (1951) 869–880. doi:10.1103/PhysRev.81.869.
1105 URL <https://link.aps.org/doi/10.1103/PhysRev.81.869>
- 1106 [10] F. J. Dyson, Thermodynamic behavior of an ideal ferromagnet, Phys.
1107 Rev. 102 (1956) 1230–1244. doi:10.1103/PhysRev.102.1230.
1108 URL <https://link.aps.org/doi/10.1103/PhysRev.102.1230>
- 1109 [11] S. Foner, A. J. Freeman, N. A. Blum, R. B. Frankel, E. J. McNiff, H. C.
1110 Praddaude, High-field studies of band ferromagnetism in Fe and Ni by
1111 Mössbauer and magnetic moment measurements, Phys. Rev. 181 (1969)
1112 863–882. doi:10.1103/PhysRev.181.863.
1113 URL <https://link.aps.org/doi/10.1103/PhysRev.181.863>
- 1114 [12] R. Pauthenet, Spinwaves in nickel, iron, and yttriumiron garnet, Journal
1115 of Applied Physics 53 (3) (1982) 2029–2031. doi:10.1063/1.330694.
1116 URL <http://dx.doi.org/10.1063/1.330694>
- 1117 [13] F. J. Dyson, General theory of spin-wave interactions, Phys. Rev. 102
1118 (1956) 1217–1230. doi:10.1103/PhysRev.102.1217.
1119 URL <https://link.aps.org/doi/10.1103/PhysRev.102.1217>
- 1120 [14] F. Keffer, Spin Waves, Springer, Berlin, Heidelberg, 1966, pp. 1–273.
1121 doi:https://doi.org/10.1007/978-3-642-46035-7_1.
- 1122 [15] R. Pauthenet, Experimental verification of spinwave theory in high fields
1123 (invited), Journal of Applied Physics 53 (11) (1982) 8187–8192. doi:
1124 10.1063/1.330287.
1125 URL <http://dx.doi.org/10.1063/1.330287>
- 1126 [16] C. D. G. Jr., Iron and nickel as magnetization standards, Journal of
1127 Applied Physics 53 (3) (1982) 2032–2034. doi:10.1063/1.330695.
1128 URL <http://dx.doi.org/10.1063/1.330695>

- 1129 [17] R. Skomski, G. C. Hadjipanayis, D. J. Sellmyer, Effective demagnetizing
1130 factors of complicated particle mixtures, *IEEE Transactions on Magnet-*
1131 *ics* 43 (6) (2007) 2956–2958. doi:10.1109/TMAG.2007.893798.
- 1132 [18] E. A. Owen, D. M. Jones, Effect of grain size on the crystal structure
1133 of cobalt, *Proceedings of the Physical Society. Section B* 67 (6) (1954)
1134 456.
1135 URL <http://stacks.iop.org/0370-1301/67/i=6/a=302>
- 1136 [19] W. E. Case, R. D. Harrington, Calibration of vibrating-sample magne-
1137 tometers, *Journal of Research of the National Bureau of Standards-C*
1138 *Engineering and Instrumentation* 70C (4) (1966) 255–262.
1139 URL [http://nvlpubs.nist.gov/nistpubs/jres/70C/](http://nvlpubs.nist.gov/nistpubs/jres/70C/jresv70Cn4p255_A1b.pdf)
1140 [jresv70Cn4p255_A1b.pdf](http://nvlpubs.nist.gov/nistpubs/jres/70C/jresv70Cn4p255_A1b.pdf)
- 1141 [20] J. Crangle, G. M. Goodman, The magnetization of pure iron and
1142 nickel, *Proceedings of the Royal Society of London A: Mathemati-*
1143 *cal, Physical and Engineering Sciences* 321 (1547) (1971) 477–491.
1144 doi:10.1098/rspa.1971.0044.
1145 URL [http://rspa.royalsocietypublishing.org/content/321/](http://rspa.royalsocietypublishing.org/content/321/1547/477)
1146 [1547/477](http://rspa.royalsocietypublishing.org/content/321/1547/477)
- 1147 [21] H. Danan, A. Herr, A. J. P. Meyer, New determinations of the saturation
1148 magnetization of nickel and iron, *Journal of Applied Physics* 39 (2)
1149 (1968) 669–670. doi:10.1063/1.2163571.
1150 URL <http://dx.doi.org/10.1063/1.2163571>
- 1151 [22] A. T. Aldred, Temperature dependence of the magnetization of nickel,
1152 *Phys. Rev. B* 11 (1975) 2597–2601. doi:10.1103/PhysRevB.11.2597.
1153 URL <https://link.aps.org/doi/10.1103/PhysRevB.11.2597>
- 1154 [23] P. Weiss, R. Forrer, La saturation absolue des ferromagnétiques et les
1155 lois d’approche en fonction du champ et de la température, *Ann. Phys.*
1156 10 (12) (1929) 279–372. doi:10.1051/anphys/192910120279.
1157 URL <https://doi.org/10.1051/anphys/192910120279>
- 1158 [24] R. L. Sanford, E. G. Bennett, A determination of the magnetic satura-
1159 tion induction of iron at room temperature, *NIST Journal of Research.*
1160 URL [http://nistdigitalarchives.contentdm.oclc.org/cdm/ref/](http://nistdigitalarchives.contentdm.oclc.org/cdm/ref/collection/p13011coll6/id/104774)
1161 [collection/p13011coll6/id/104774](http://nistdigitalarchives.contentdm.oclc.org/cdm/ref/collection/p13011coll6/id/104774)

- 1162 [25] H. Danan, On the interpretation of the magnetization measurements
1163 of pure polycrystalline iron and nickel in the vicinity of saturation,
1164 J. Phys. Radium 20 (2-3) (1959) 203–207. doi:10.1051/jphysrad:
1165 01959002002-3020300.
1166 URL <https://hal.archives-ouvertes.fr/jpa-00236018>
- 1167 [26] S. Arajs, G. R. Dunmyre, A note on the consistency of values of the
1168 spontaneous or saturation magnetization of polycrystalline iron and
1169 nickel at 298 °K, Physica Status Solidi (b) 21 (1) (1967) 191–195.
1170 doi:10.1002/pssb.19670210117.
1171 URL <http://dx.doi.org/10.1002/pssb.19670210117>
- 1172 [27] D. R. Behrendt, D. E. Hegland, Saturation magnetization of polycrys-
1173 talline iron, Tech. rep., NASA (Apr 1972).
1174 URL <https://ntrs.nasa.gov/search.jsp?R=19720015089>
- 1175 [28] C. S. Edmund, Ferromagnetism: magnetization curves, Reports on
1176 Progress in Physics 13 (1) (1950) 83–183. doi:10.1088/0034-4885/
1177 13/1/304.
1178 URL <https://doi.org/10.1088/0034-4885/13/1/304>
- 1179 [29] S. Foner, Hall effect and magnetic properties of armco iron, Phys. Rev.
1180 101 (1956) 1648–1652. doi:10.1103/PhysRev.101.1648.
1181 URL <https://link.aps.org/doi/10.1103/PhysRev.101.1648>
- 1182 [30] B. D. Cullity, C. D. Graham, Introduction to Magnetic Materials, 2nd
1183 Edition, Wiley-IEEE Press, 2008.
- 1184 [31] H. P. Myers, W. Sucksmith, The spontaneous magnetization of
1185 cobalt, Proceedings of the Royal Society of London A: Mathemat-
1186 ical, Physical and Engineering Sciences 207 (1091) (1951) 427–446.
1187 arXiv:[http://rspa.royalsocietypublishing.org/content/207/](http://rspa.royalsocietypublishing.org/content/207/1091/427.full.pdf)
1188 [1091/427.full.pdf](http://rspa.royalsocietypublishing.org/content/207/1091/427.full.pdf), doi:10.1098/rspa.1951.0132.
1189 URL [http://rspa.royalsocietypublishing.org/content/207/](http://rspa.royalsocietypublishing.org/content/207/1091/427)
1190 [1091/427](http://rspa.royalsocietypublishing.org/content/207/1091/427)
- 1191 [32] S. Arajs, R. V. Colvin, Ferromagneticparamagnetic transition in iron,
1192 Journal of Applied Physics 35 (8) (1964) 2424–2426. doi:10.1063/1.
1193 1702873.
1194 URL <http://dx.doi.org/10.1063/1.1702873>

- 1195 [33] S. Arajs, R. Colvin, Paramagnetism of polycrystalline nickel, Journal
1196 of Physics and Chemistry of Solids 24 (10) (1963) 1233 – 1237.
1197 doi:[http://dx.doi.org/10.1016/0022-3697\(63\)90242-7](http://dx.doi.org/10.1016/0022-3697(63)90242-7).
1198 URL [http://www.sciencedirect.com/science/article/pii/](http://www.sciencedirect.com/science/article/pii/0022369763902427)
1199 0022369763902427
- 1200 [34] S. Arajs, Paramagnetic behavior of nickel just above the ferromagnetic
1201 curie temperature, Journal of Applied Physics 36 (3) (1965) 1136–1137.
1202 doi:10.1063/1.1714136.
1203 URL <http://dx.doi.org/10.1063/1.1714136>
- 1204 [35] F. E. Luborsky, J. L. Walter, E. P. Wohlfarth, The saturation mag-
1205 netisation, curie temperature and size effect of amorphous iron alloys,
1206 Journal of Physics F: Metal Physics 10 (5) (1980) 959.
1207 URL <http://stacks.iop.org/0305-4608/10/i=5/a=024>
- 1208 [36] S. A. Ahern, M. J. C. Martin, W. Sucksmith, The spontaneous mag-
1209 netization of nickel+copper alloys, Proceedings of the Royal Society of
1210 London. Series A, Mathematical and Physical Sciences 248 (1253) (1958)
1211 145–152.
1212 URL <http://www.jstor.org/stable/100593>
- 1213 [37] P. R. Locher, S. Geschwind, Electron-nuclear double resonance of Fe⁵⁷
1214 in MgO, Phys. Rev. 139 (1965) A991–A994. doi:10.1103/PhysRev.
1215 139.A991.
1216 URL <https://link.aps.org/doi/10.1103/PhysRev.139.A991>
- 1217 [38] O. W. Richardson, A mechanical effect accompanying magnetiza-
1218 tion, Phys. Rev. (Series I) 26 (1908) 248–253. doi:10.1103/
1219 PhysRevSeriesI.26.248.
1220 URL <https://link.aps.org/doi/10.1103/PhysRevSeriesI.26.248>
- 1221 [39] G. G. Scott, Review of Gyromagnetic Ratio Experiments, Reviews of
1222 Modern Physics 34 (1962) 102–109. doi:10.1103/RevModPhys.34.102.
- 1223 [40] S. J. Barnett, On magnetization by angular acceleration (Sep. 1909).
1224 doi:10.1126/science.30.769.413.
1225 URL <https://doi.org/10.1126/science.30.769.413>

- 1226 [41] S. J. Barnett, New researches on magnetization by rotation and the gy-
1227 romagnetic ratios of ferromagnetic substances, Proceedings of the Amer-
1228 ican Academy of Arts and Sciences 75 (5) (1944) 109–129.
1229 URL <http://www.jstor.org/stable/20023462>
- 1230 [42] C. Kittel, On the gyromagnetic ratio and spectroscopic splitting factor
1231 of ferromagnetic substances, Phys. Rev. 76 (1949) 743–748. doi:10.
1232 1103/PhysRev.76.743.
1233 URL <https://link.aps.org/doi/10.1103/PhysRev.76.743>
- 1234 [43] A. J. P. Meyer, G. Asch, Experimental g' and g values of Fe, Co, Ni,
1235 and their alloys, Journal of Applied Physics 32 (3) (1961) S330–S333.
1236 doi:10.1063/1.2000457.
1237 URL <http://dx.doi.org/10.1063/1.2000457>
- 1238 [44] J. Smit, H. Wijn, Ferrites, Eindhoven: Philips Technical Library, 1959.
- 1239 [45] M. Phillips, The effect of nuclear motion on atomic magnetic moments,
1240 Phys. Rev. 76 (1949) 1803–1804. doi:10.1103/PhysRev.76.1803.
1241 URL <https://link.aps.org/doi/10.1103/PhysRev.76.1803>
- 1242 [46] G. G. Scott, A precise mechanical measurement of the gyromagnetic
1243 ratio of iron, Phys. Rev. 82 (1951) 542–547. doi:10.1103/PhysRev.
1244 82.542.
1245 URL <https://link.aps.org/doi/10.1103/PhysRev.82.542>
- 1246 [47] S. J. Barnett, G. S. Kenny, Gyromagnetic ratios of iron, cobalt, and
1247 many binary alloys of iron, cobalt, and nickel, Phys. Rev. 87 (1952)
1248 723–734. doi:10.1103/PhysRev.87.723.
1249 URL <https://link.aps.org/doi/10.1103/PhysRev.87.723>
- 1250 [48] Meyer, Andr J.P., Brown, Sheldon, Nouvelles mesures des rapports gy-
1251 romagntiques du fer et du nickel, J. Phys. Radium 18 (3) (1957) 161–168.
1252 doi:10.1051/jphysrad:01957001803016100.
1253 URL <https://doi.org/10.1051/jphysrad:01957001803016100>
- 1254 [49] G. G. Scott, Gyromagnetic ratios of Fe and Ni, Phys. Rev. 119 (1960)
1255 84–85. doi:10.1103/PhysRev.119.84.
1256 URL <https://link.aps.org/doi/10.1103/PhysRev.119.84>

- 1257 [50] E. Wohlfarth, Chapter 1 iron, cobalt and nickel, Handbook of Ferro-
1258 magnetic Materials 1 (1980) 35. doi:[http://dx.doi.org/10.1016/](http://dx.doi.org/10.1016/S1574-9304(05)80116-6)
1259 [S1574-9304\(05\)80116-6](http://dx.doi.org/10.1016/S1574-9304(05)80116-6).
1260 URL [http://www.sciencedirect.com/science/article/pii/](http://www.sciencedirect.com/science/article/pii/S1574930405801166)
1261 [S1574930405801166](http://www.sciencedirect.com/science/article/pii/S1574930405801166)
- 1262 [51] D. Bonnenberg, K. A. Hempel, H. Wijn, 1.2.1.2.4 Atomic magnetic mo-
1263 ment, magnetic moment density, g and g' factor, Springer Berlin Heidel-
1264 berg, Berlin, Heidelberg, 1986, pp. 174–188. doi:[10.1007/10311893_](https://doi.org/10.1007/10311893_25)
1265 [25](https://doi.org/10.1007/10311893_25).
1266 URL https://doi.org/10.1007/10311893_25
- 1267 [52] G. G. Scott, H. W. Sturmer, Magnetomechanical ratios for Fe-Co alloys,
1268 Phys. Rev. 184 (1969) 490–491. doi:[10.1103/PhysRev.184.490](https://link.aps.org/doi/10.1103/PhysRev.184.490).
1269 URL <https://link.aps.org/doi/10.1103/PhysRev.184.490>
- 1270 [53] L. Pst, Z. Frait, Low-temperature FMR and FMAR measurements of
1271 tetal single crystals. I. General Consideration, Experimental Techniques,
1272 Physica Status Solidi (b) 122 (2) (1984) 535–541. doi:[10.1002/pssb.](https://doi.org/10.1002/pssb.2221220218)
1273 [2221220218](https://doi.org/10.1002/pssb.2221220218).
1274 URL <http://dx.doi.org/10.1002/pssb.2221220218>
- 1275 [54] M. *et al.* Tanabashi, Review of particle physics, Phys. Rev. D 98 (2018)
1276 030001. doi:[10.1103/PhysRevD.98.030001](https://link.aps.org/doi/10.1103/PhysRevD.98.030001).
1277 URL <https://link.aps.org/doi/10.1103/PhysRevD.98.030001>
- 1278 [55] J. H. Van Vleck, Concerning the theory of ferromagnetic resonance ab-
1279 sorption, Phys. Rev. 78 (1950) 266–274. doi:[10.1103/PhysRev.78.266](https://link.aps.org/doi/10.1103/PhysRev.78.266).
1280 URL <https://link.aps.org/doi/10.1103/PhysRev.78.266>
- 1281 [56] R. A. Reck, D. L. Fry, Orbital and spin magnetization in Fe-Co, Fe-
1282 Ni, and Ni-Co, Phys. Rev. 184 (1969) 492–495. doi:[10.1103/PhysRev.](https://link.aps.org/doi/10.1103/PhysRev.184.492)
1283 [184.492](https://link.aps.org/doi/10.1103/PhysRev.184.492).
1284 URL <https://link.aps.org/doi/10.1103/PhysRev.184.492>
- 1285 [57] G. G. Scott, Gyromagnetic ratio of nickel at low magnetic intensities,
1286 Phys. Rev. 99 (1955) 1824–1825. doi:[10.1103/PhysRev.99.1824](https://link.aps.org/doi/10.1103/PhysRev.99.1824).
1287 URL <https://link.aps.org/doi/10.1103/PhysRev.99.1824>
- 1288 [58] K. J. Standley, K. H. Reich, Ferromagnetic resonance in nickel and in
1289 some of its alloys, Proceedings of the Physical Society. Section B 68 (10)

- 1290 (1955) 713.
1291 URL <http://stacks.iop.org/0370-1301/68/i=10/a=303>
- 1292 [59] A. Borovik-Romanov, S. Sinha, Spin Waves and Magnetic Excitations,
1293 no. 2 in Modern problems in condensed matter sciences, North-Holland,
1294 1988.
1295 URL <https://books.google.com/books?id=Qj9BAQAAIAAJ>
- 1296 [60] C. J. Gadsden, M. Heath, Ferromagnetic resonance of nickel vanadium
1297 alloys, Journal of Physics F: Metal Physics 8 (3) (1978) 521.
1298 URL <http://stacks.iop.org/0305-4608/8/i=3/a=021>
- 1299 [61] B. D. Shanina, V. G. Gavriljuk, A. A. Konchits, S. P. Kolesnik, The
1300 influence of substitutional atoms upon the electron structure of the iron-
1301 based transition metal alloys, Journal of Physics: Condensed Matter
1302 10 (8) (1998) 1825.
1303 URL <http://stacks.iop.org/0953-8984/10/i=8/a=015>
- 1304 [62] G. Dewar, B. Heinrich, J. F. Cochran, Ferromagnetic antiresonance
1305 transmission of 24ghz radiation through nickel (20 to 364 c), Canadian
1306 Journal of Physics 55 (9) (1977) 821–833. doi:10.1139/p77-112.
1307 URL <https://doi.org/10.1139/p77-112>
- 1308 [63] L. Pst, Z. Frait, Precise g-factor determination of Fe-3wt%Si single
1309 crystals in the temperature range 3.5 - 300 K by electron FMR
1310 and FMAR measurements, Physics Letters A 86 (1) (1981) 48 – 50.
1311 doi:[http://dx.doi.org/10.1016/0375-9601\(81\)90685-X](http://dx.doi.org/10.1016/0375-9601(81)90685-X).
1312 URL [http://www.sciencedirect.com/science/article/pii/](http://www.sciencedirect.com/science/article/pii/037596018190685X)
1313 [037596018190685X](http://www.sciencedirect.com/science/article/pii/037596018190685X)
- 1314 [64] S. Haraldson, L. Pettersson, Ferromagnetic resonance in nickel around
1315 the curie temperature, Journal of Physics and Chemistry of Solids 42 (8)
1316 (1981) 681 – 686. doi:[http://dx.doi.org/10.1016/0022-3697\(81\)](http://dx.doi.org/10.1016/0022-3697(81)90121-9)
1317 [90121-9](http://dx.doi.org/10.1016/0022-3697(81)90121-9).
1318 URL [http://www.sciencedirect.com/science/article/pii/](http://www.sciencedirect.com/science/article/pii/0022369781901219)
1319 [0022369781901219](http://www.sciencedirect.com/science/article/pii/0022369781901219)
- 1320 [65] D. Bastian, E. Biller, Anisotropy constants and g-factors of NiFe alloys
1321 derived from ferromagnetic resonance, physica status solidi (a) 35 (2)

- 1322 (1976) 465–470. doi:10.1002/pssa.2210350207.
 1323 URL <http://dx.doi.org/10.1002/pssa.2210350207>
- 1324 [66] D. S. Rodbell, Ferromagnetic resonance absorption linewidth of nickel
 1325 metal. Evidence for Landau-Lifshitz damping, Phys. Rev. Lett. 13 (1964)
 1326 471–474. doi:10.1103/PhysRevLett.13.471.
 1327 URL <https://link.aps.org/doi/10.1103/PhysRevLett.13.471>
- 1328 [67] D. S. Rodbell, Ferromagnetic resonance of iron whisker crystals, Journal
 1329 of Applied Physics 30 (4) (1959) S187–S188. doi:10.1063/1.2185880.
 1330 URL <http://dx.doi.org/10.1063/1.2185880>
- 1331 [68] D. M. S. Bagguley, N. J. Harrick, The temperature dependence of fer-
 1332 romagnetic resonance in colloidal nickel, Proceedings of the Physical
 1333 Society. Section A 67 (7) (1954) 648.
 1334 URL <http://stacks.iop.org/0370-1298/67/i=7/a=115>
- 1335 [69] N. Bloembergen, On the ferromagnetic resonance in nickel and su-
 1336 permalloy, Phys. Rev. 78 (1950) 572–580. doi:10.1103/PhysRev.78.
 1337 572.
 1338 URL <https://link.aps.org/doi/10.1103/PhysRev.78.572>
- 1339 [70] G. G. Scott, Gyromagnetic ratio of iron at low magnetic intensities,
 1340 Phys. Rev. 99 (1955) 1241–1244. doi:10.1103/PhysRev.99.1241.
 1341 URL <https://link.aps.org/doi/10.1103/PhysRev.99.1241>
- 1342 [71] G. G. Scott, Gyromagnetic ratios of the iron-nickel alloys, Phys. Rev.
 1343 103 (1956) 561–563. doi:10.1103/PhysRev.103.561.
 1344 URL <https://link.aps.org/doi/10.1103/PhysRev.103.561>
- 1345 [72] FRAIT, Z., GEMPERLE, R., The g-factor and surface magnetization
 1346 of pure iron along [100] and [111] directions, J. Phys. Colloques 32.
 1347 doi:10.1051/jphyscol:19711182.
 1348 URL <https://doi.org/10.1051/jphyscol:19711182>
- 1349 [73] C. Kittel, On the theory of ferromagnetic resonance absorption, Phys.
 1350 Rev. 73 (1948) 155–161. doi:10.1103/PhysRev.73.155.
 1351 URL <https://link.aps.org/doi/10.1103/PhysRev.73.155>

- 1352 [74] Z. Frait, The g-factor in pure polycrystalline iron, Czechoslovak Journal
1353 of Physics B 27 (2) (1977) 185–189. doi:10.1007/BF01587010.
1354 URL <https://doi.org/10.1007/BF01587010>
- 1355 [75] Z. Frait, H. MacFaden, Ferromagnetic resonance in metals. Frequency
1356 dependence, Phys. Rev. 139 (1965) A1173–A1181. doi:10.1103/
1357 PhysRev.139.A1173.
1358 URL <https://link.aps.org/doi/10.1103/PhysRev.139.A1173>
- 1359 [76] C. Herring, R. M. Bozorth, A. E. Clark, T. R. McGuire, Highfield sus-
1360 ceptibilities of iron and nickel, Journal of Applied Physics 37 (3) (1966)
1361 1340–1341. arXiv:<https://doi.org/10.1063/1.1708462>, doi:10.
1362 1063/1.1708462.
1363 URL <https://doi.org/10.1063/1.1708462>
- 1364 [77] J. Stoelinga, R. Gersdorf, Field dependence of the magnetization in high
1365 fields for bcc fe-co and fe-ni alloys, Physics Letters 19 (8) (1966) 640–641.
- 1366 [78] M. Yasui, M. Shimizu, Calculations of orbital paramagnetic susceptibil-
1367 ity for vanadium, chromium and iron, Journal of the Physical Society
1368 of Japan 31 (2) (1971) 378–381. arXiv:<https://doi.org/10.1143/JPSJ.31.378>,
1369 JPSJ.31.378, doi:10.1143/JPSJ.31.378.
1370 URL <https://doi.org/10.1143/JPSJ.31.378>
- 1371 [79] A. J. Freeman, N. A. Blum, S. Foner, R. B. Frankel, E. J. Mc-
1372 Niff, Ferromagnetic metals in high magnetic fields, Journal of Applied
1373 Physics 37 (3) (1966) 1338–1339. arXiv:[https://doi.org/10.1063/](https://doi.org/10.1063/1.1708461)
1374 [1.1708461](https://doi.org/10.1063/1.1708461), doi:10.1063/1.1708461.
1375 URL <https://doi.org/10.1063/1.1708461>